Electronic Supplementary Material (ESI) for ChemComm.

Supporting Information

Gauging the donor strength of iron(0) complexes via their N-heterocyclic carbene gold(I) adducts

Zhi Hao Toh,[a] Hendrik Tinnermann,[a] Dinh Cao Huan Do,[a] Han Vinh Huynh,[a] Tobias Krämer,[b] Rowan D. Young*[a]

[a] *Department of Chemistry, National University of Singapore, 3 Science Drive 3, Singapore 117543*

[b] *Department of Chemistry, Maynooth University, Maynooth, Co. Kildare, Ireland*

**Corresponding Author*

Table of Contents

Experimental

General information

All syntheses were carried out in N_2 atmosphere using a glovebox or with standard Schlenk techniques. Complex **1** was prepared according to a reported method.[1] Toluene, DCM and hexanes were dried over activated alumina using a LC Technology Solutions Inc. SP-1 solvent purification system and then deoxygenated prior to use. C_6D_6, CD_2Cl_2 and fluorobenzene were stirred over CaH_2 at room temperature under a nitrogen atmosphere overnight prior to distillation under reduced pressure and storage over 4 Å molecular sieves. NMR spectra were recorded using Bruker AV500 and DRX500 spectrometers. All chemical shifts are quoted in parts per million (ppm) relative to solvent (DCM-d_2: ^{1}H NMR 5.35 ppm, ^{13}C NMR 53.84 ppm; $CDCl_3$: ^{1}H NMR 7.26 ppm, ^{13}C NMR 77.7 ppm)[1] or H_3PO_4 (85%) (^{31}P). Coupling constant *J* values are given in Hz. ^{13}C and ^{31}P NMR analyses were performed with ^{1}H decoupling. HRMS (ESI-TOF) spectra were obtained using an Agilent 6546 LC-QTOF. Single crystal data were measured at low temperature (T = 100K) on a four circles goniometer Kappa geometry Bruker AXS D8 Venture equipped with a Photon 100 CMOS active pixel sensor detector using molybdenum monochromatized (λ = 0.71073 Å) X-Ray radiation. Structures were deposited in the Cambridge Crystallographic Data Centre (CCDC) (**2a** 2206892 and **[Au(1a)$_2$][BAr$^F_4$]** 2206893). Elemental analyses were obtained by the National University of Singapore's Chemical, Molecular and Materials Analysis Centre (CMMAC).

Compounds **1**, (^{i}Pr$_2$-bimy)AuCl, [^{13}C](^{i}Pr$_2$-bimy)AuCl {^{i}Pr$_2$-bimy = 1,3-diisopropylbenzimidazolin-2-ylidene} and Na[BAr$^F_4$] {BAr$^F_4$ = tetrakis(pentafluorophenyl)borate} were prepared according to literature reports.[2] All other reagents were purchased form commercial sources and used as received.

Preparation of complex 2a

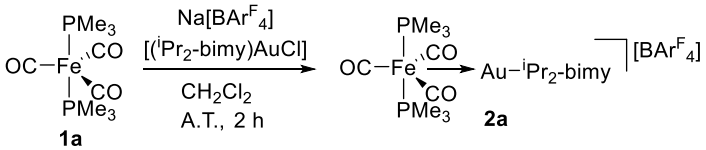

Complex **1a** (12.2 mg, 0.04 mmol) and Na[BAr$^F_4$] (13.0 mg, 0.03 mmol) were mixed in CH_2Cl_2 in a glass vial. In a separate glass vial, [(^{i}Pr$_2$-bimy)AuCl] (21.0 mg, 0.03 mmol) was dissolved in CH_2Cl_2. The latter solution was then added to the former via a glass pipette, and the resulting suspension was filtered to remove solid particulates. The resulting solution was then layered with *n*-hexane. The initial crystallization (7.3 mg) gave

predominantly [Au(**1a**)$_2$][BAr$^F_4$] (see below), while layering with additional *n*-hexane produced a second crop of crystals (20.5 mg) with a 94% NMR purity of the desired product (19.2 mg, 47%).

^{1}H NMR (500 MHz, CD_2Cl_2, 298 K) = δ_H 1.68 (d, $^2J_{PH}$ = 8.3 Hz, 18 H), 1.77 (d, $^3J_{HH}$ = 6.9 Hz, 12 H), 5.34 (sept, $^3J_{HH}$ = 6.9 Hz), 7.42-7.47 (m, 2 H), 7.67-7.72 (m, 2 H); ^{13}C{^{1}H} NMR (126 MHz, CD_2Cl_2, 298 K) = δ_C 22.1 (s, 4 C), 22.3 (d, $^1J_{PC}$ = 15.0 Hz, 2 C), 54.4 (s, 2 C), 113.6 (s, 2 C), 124.3 (br, 4 C), 125.0 (s, 2 C), 132.7 (s, 2 C), 136.6 (d, *J* = 244 Hz, 8 C), 138.6 (d, *J* = 244 Hz, 4 C), 148.5 (d, *J* = 243 Hz, 8 C), 190.1 (t, *J* = 4.7 Hz), 1 C), 209.2 (br, 1 C), 215.2 (t, *J* = 24.1, 2 C); ^{31}P{^{1}H} NMR (202 MHz, CD_2Cl_2, 298 K) = δ_P 24.7 (s, 2 P); ^{19}F{^{1}H} NMR (470 MHz, CD_2Cl_2, 298 K) = δ_F -133.0 (s, 8 F), -163.8 (s, 4 F), -167.5 (s, 8 F); ^{11}B{^{1}H} NMR (160 MHz, CD_2Cl_2, 298 K) = δ_B -16.8 (s, 1 B); FTIR (CH_2Cl_2) ν_{CO}: 2005, 1946, 1923 cm^{-1}; HRMS (ESI-TOF) m/z: [M]$^+$ Calcd for $C_{22}H_{36}AuFeN_2O_3P_2$ 689.1257; Found 689.1255

Independent synthesis of [Au(1a)$_2$][BAr$^F_4$]

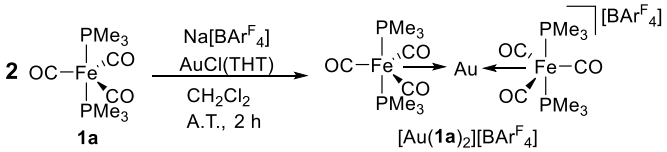

Complex **1a** (15.4 mg, 0.052 mmol) and Na[BAr$^F_4$] (14.4 mg, 0.02 mmol) were mixed in CH_2Cl_2 in a glass vial. In a separate glass vial, [(THT)AuCl] (6.4 mg, 0.02 mmol) was dissolved in CH_2Cl_2. The latter solution was then added to the former via a glass pipette, and the resulting suspension was filtered to remove solid particulates. The resulting solution was subjected to slow evaporation to remove the solvent. The crude product was washed thoroughly with *n*-hexane to remove residual complex **1a** starting material. [Au(**1a**)$_2$][BAr$^F_4$] was isolated in 65% yield (19 mg) and X-ray quality crystals were produced by recrystallisation in DCM/*n*-hexane solvent mixture at -10 °C.

^{1}H NMR (500 MHz, CD_2Cl_2, 298 K) = δ_H 1.69 (d, *J* = 7.7 Hz, 36 H); ^{13}C{^{1}H} NMR (126 MHz, CD_2Cl_2, 298 K) = δ_C 22.2 (AA'X spin system, J_{AX} = -34 Hz, $J_{A'X}$ = 0.6 Hz, $J_{AA'}$ = 30 Hz, 4 P), 124.2 (br, 4 C), 136.7 (d, *J* = 237 Hz, 8 C), 138.7 (d, *J* = 242 Hz, 4 C), 148.5 (d, *J* = 242 Hz, 8 C), 210.3 (br, 2 C), 216.5 (t, *J* = 24.5 Hz, 4 C). ^{31}P{^{1}H} NMR (202 MHz, CD_2Cl_2, 298 K) = δ_P 19.5 (s, 4 P); ^{19}F{^{1}H} NMR (470 MHz, CD_2Cl_2, 298 K) = δ_F -133.0 (s, 8 F), -163.8 (s, 4 F), -167.5 (s, 8 F); ^{11}B{^{1}H} NMR (160 MHz, CD_2Cl_2, 298 K) = δ_B -16.8 (s, 1 B); HRMS (ESI-TOF) m/z: [M]$^+$ Calcd for $C_{18}H_{36}AuFe_2O_6P_4$ 780.9821; Found 780.9824; Found: C, 34.68; H, 2.46. Calc. for $C_{42}H_{36}AuBF_{20}Fe_2O_6P_4$: C, 34.55; H, 2.49%.

Independent synthesis of [Au(^{i}Pr$_2$-bimy)$_2$][BAr$^F_4$]

The synthesis of the salt **[(^{i}Pr$_2$-bimy)H][BAr$^F_4$]** and the complex **[Au(^{i}Pr$_2$-bimy)$_2$][BAr$^F_4$]** was based on the procedure reported by Jothibasu *et al*. for the $[BF_4]^-$ analogues.[2e]

[(^{i}Pr$_2$-bimy)H][BAr$^F_4$]: [(^{i}Pr$_2$-bimy)H]Br (100 mg, 0.35 mmol, 1 equiv.) and Na[BAr$^F_4$] (249 mg, 0.35 mmol, 1 equiv.) were suspended in acetone (10 mL) and stirred at ambient conditions. Filtration, followed by removal of volatiles *in vacuo* afforded a sticky off-white solid. To this residue THF (1 mL) was added, and the resulting mixture was sonicated vigorously. Removal of the liquid portion and drying of the remaining solid afforded the crude product as a white powder, which was sufficiently (and spectroscopically) pure for the subsequent step. Yield 241 mg, 78%. ^{1}H NMR (400 MHz, $CDCl_3$): δ = 8.46 (s, 1H, NC<u>H</u>N), 7.69 – 7.76 (overlapping multiplets, 4H, Ar–H), 4.87 (sept, J_{HH} = 6.7 Hz, 2H, C<u>H</u>(CH$_3$)), 1.69 (d, J_{HH} = 6.7 Hz, 12H, CH(C<u>H</u>$_3$)). ^{13}C{^{1}H} NMR (101 MHz, $CDCl_3$): 148.7 (d, C_6F_5-C J_{CF} = 241.2 Hz), 138.6 (d, C_6F_5-C J_{CF} = 246.1 Hz), 136.9 (d, C_6F_5-C J_{CF} = 245.4 Hz), 134.2 (s, N<u>C</u>HN), 131.7, 128.9, (s, Ar–C), 124.8 (br s, B–C), 114.2 (s, Ar–C), 52.7 (s, <u>C</u>H(CH$_3$)), 22.3 (s, CH(<u>C</u>H$_3$)). ^{11}B NMR (128 MHz, $CDCl_3$): δ = -16.7. ^{19}F NMR (376 MHz, $CDCl_3$): δ = -132.6 (d, J_{FF} = 10 Hz), -162.7 (t, J_{FF} = 20 Hz), -166.8 (t, J_{FF} = 20 Hz).

[Au(^{i}Pr$_2$-bimy)$_2$][BAr$^F_4$]: K_2CO_3 (21 mg, 0.15 mmol, 1.3 equiv.) was added to the mixture of [AuCl(^{i}Pr$_2$-bimy)] (49 mg, 0.11 mmol, 1 equiv.) and [(^{i}Pr$_2$-bimy)H][BAr$^F_4$] (100 mg, 0.11 mmol, 1 equiv.) in acetone (20 ml). After a reaction time of 24 h according to the reported procedure, volatiles were removed *in vacuo*. DCM (10 ml) was then added to the residue, and filration through celite, followed by removal of solvent *in vacuo*, afforded the crude solid, which was partially soluble in EtOAc. ^{1}H NMR spectroscopy data of this solid suggested a mixture of unreacted [(^{i}Pr$_2$-bimy)H][BAr$^F_4$] and [AuCl(^{i}Pr$_2$-bimy)], as well as the desired product. [AuCl(^{i}Pr$_2$-bimy)] was first separated by column chromatography (eluent 100 % EtOAc, R_F = 0.72), and [Au(^{i}Pr$_2$-bimy)$_2$][BAr$^F_4$] was subsequently isolated (eluent 100% DCM, R_F = 0.64) as a white solid. Yield 8.5 mg, 6% (*unoptimised*). ^{1}H NMR (400 MHz, $CDCl_3$): δ = 7.69 (dd, 4H, Ar–H, J_{HH} = 3.2 and 6.3 Hz), 7.46 (dd, 4H, Ar–H, J_{HH} = 3.2 and 6.3 Hz), 5.34 (sept, J_{HH} = 7.0 Hz, 4H, C<u>H</u>(CH$_3$)), 1.83 (d, J_{HH} = 7.0 Hz, 24H, CH(C<u>H</u>$_3$)). ^{13}C{^{1}H} NMR (125 MHz, $CDCl_3$): δ = 187.3 (s, $C_{carbene}$), 148.8 (d, C_6F_5-C J_{CF} = 240.9 Hz), 135.8 – 139.9 (overlapping signals, C_6F_5-C), 133.2, 125.6 (s, Ar–C), 124.7 (br s, B–C), 113.7 (s, Ar–C), 54.5 (s, <u>C</u>H(CH$_3$)), 23.0 (s, CH(<u>C</u>H$_3$)). ^{11}B NMR (128 MHz, $CDCl_3$): δ = -16.7. ^{19}F NMR (376 MHz, $CDCl_3$): δ = -132.6 (d, $^3J_{FF}$ = 10 Hz), -

163.4 (t, J_{FF} = 20 Hz), -167.0 (t, J_{FF} = 20 Hz). HRMS (ESI-TOF): *m*/*z* calc. for $C_{26}H_{36}AuN_4$ ([M-B(C_6F_5)$_4$]$^+$) 601.2605, meas. 601.2604.

General procedure for *in situ* formation of [(^{i}Pr$_2$-bimy)Au-Fe(CO)$_3$(PR$_3$)$_2$] (PR$_3$ = PMe$_3$, PPh$_3$, PCy$_3$, PCyPh$_2$, PMePh$_2$, P(4-C$_6$H$_4$F)$_3$) (2a-h) and measurement of carbenic ^{13}C NMR signal

Note: to allow fast ^{13}C NMR acquisition, ^{13}C isotopically enriched ^{i}Pr$_2$-bimy (^{13}C enriched at the carbene carbon position)[2c] was utilised for *in situ* syntheses of all complexes except **2a** and **2d**. Reactions were conducted with 0.01 mmol to 0.1 mmol of starting material reagents.

Example: Complex **1g** Fe(CO)$_3$(P(4-C$_6$H$_4$F)$_3$)$_2$] (11.6 mg, 0.015 mmol) and Na[BAr$^F{}_4$] (7.0 mg, 0.01 mmol) were mixed in CD_2Cl_2 (0.2 mL) in a glass vial. In a separate glass vial, [([^{13}C]^{i}Pr$_2$-bimy)AuCl] (4.4 mg, 0.01 mmol) was dissolved in CD_2Cl_2 (0.2 mL) The latter solution was then added to the former via a glass pipette. The resulting mixture was filtered to remove solid particulates into a J. Young valve NMR tube and mixed (rotated) at room temperature for 1 hour. The solution was then analysed by ^{31}P and ^{13}C NMR spectroscopy. The product's ^{31}P NMR and ^{13}C NMR reporter signals were identified by their characteristic ^{13}C-^{31}P coupling.

Select *in situ* characterisation data for compounds 2a-h

[(^{i}Pr$_2$-bimy)Au-Fe(CO)$_3$(PMe$_3$)$_2$] (2a) ^{31}P{^{1}H} NMR (202 MHz, CD_2Cl_2, 298 K) = δ_P 24.7 (s); ^{13}C{^{1}H} NMR (126 MHz, CD_2Cl_2, 298 K) = δ_C 190.1 (t, $^3J_{CP}$ = 4.7 Hz); (126 MHz, $CDCl_3$, 298 K) = δ_C 190.0 (t, $^3J_{CP}$ = 4.7 Hz).

[([^{13}C]^{i}Pr$_2$-bimy)Au-Fe(CO)$_3$(PPh$_3$)$_2$] (2b) ^{31}P{^{1}H} NMR (202 MHz, CD_2Cl_2, 298 K) = δ_P 66.3 (d, $^3J_{CP}$ = 4.3 Hz); ^{13}C{^{1}H} NMR (126 MHz, CD_2Cl_2, 298 K) = δ_C 188.2 (t, $^3J_{CP}$ = 4.3 Hz).

[([^{13}C]^{i}Pr$_2$-bimy)Au-Fe(CO)$_3$(PCy$_3$)$_2$] (2c) ^{31}P{^{1}H} NMR (202 MHz, CD_2Cl_2, 298 K) = δ_P 74.9 (d, $^3J_{CP}$ = 3.5 Hz); ^{13}C{^{1}H} NMR (126 MHz, CD_2Cl_2, 298 K) = δ_C 190.7 (t, $^3J_{CP}$ = 3.5 Hz).

[(^{i}Pr$_2$-bimy)Au-Fe(CO)$_3$(PMePh$_2$)$_2$] (2d) ^{31}P{^{1}H} NMR (202 MHz, CD_2Cl_2, 298 K) = δ_P 44.5 (s); ^{13}C{^{1}H} NMR (126 MHz, CD_2Cl_2, 298 K) = δ_C 188.4 (t, $^3J_{CP}$ = 4.6 Hz).

[([^{13}C]^{i}Pr$_2$-bimy)Au-Fe(CO)$_3$(PMe$_2$Ph)$_2$] (2e) ^{31}P{^{1}H} NMR (202 MHz, CD_2Cl_2, 298 K) = δ_P 31.6 (d, $^3J_{CP}$ = 4.7 Hz); ^{13}C{^{1}H} NMR (126 MHz, CD_2Cl_2, 298 K) = δ_C 189.5 (t, $^3J_{CP}$ = 4.7 Hz)..

[([^{13}C]^{i}Pr$_2$-bimy)Au-Fe(CO)$_3$(PCyPh$_2$)$_2$] (2f) ^{31}P{^{1}H} NMR (202 MHz, CD_2Cl_2, 298 K) = δ_P 67.3 (d, $^3J_{CP}$ = 4.3 Hz); ^{13}C{^{1}H} NMR (126 MHz, CD_2Cl_2, 298 K) = δ_C 189.2 (t, $^3J_{CP}$ = 4.3 Hz).

[([^{13}C]^{i}Pr$_2$-bimy)Au-Fe(CO)$_3$(P(4-C$_6$H$_4$F)$_3$)$_2$] (2g) ^{31}P{^{1}H} NMR (202 MHz, CD_2Cl_2, 298 K) = δ_P 64.3 (d, $^{3}J_{CP}$ = 4.4 Hz); ^{13}C{^{1}H} NMR (126 MHz, CD_2Cl_2, 298 K) = δ_C 187.0 (t, $^{3}J_{PC}$ = 4.4 Hz).

[([^{13}C]^{i}Pr$_2$-bimy)Au-Fe(CO)$_4$(PPh$_3$)] (2h) ^{31}P{^{1}H} NMR (202 MHz, CD_2Cl_2, 298 K) = δ_P 56.0 (d, $^{3}J_{CP}$ = 2.9 Hz) ^{13}C{^{1}H} NMR (126 MHz, CD_2Cl_2, 298 K) = δ_C 185.4 (d, $^{3}J_{CP}$ = 2.9 Hz).

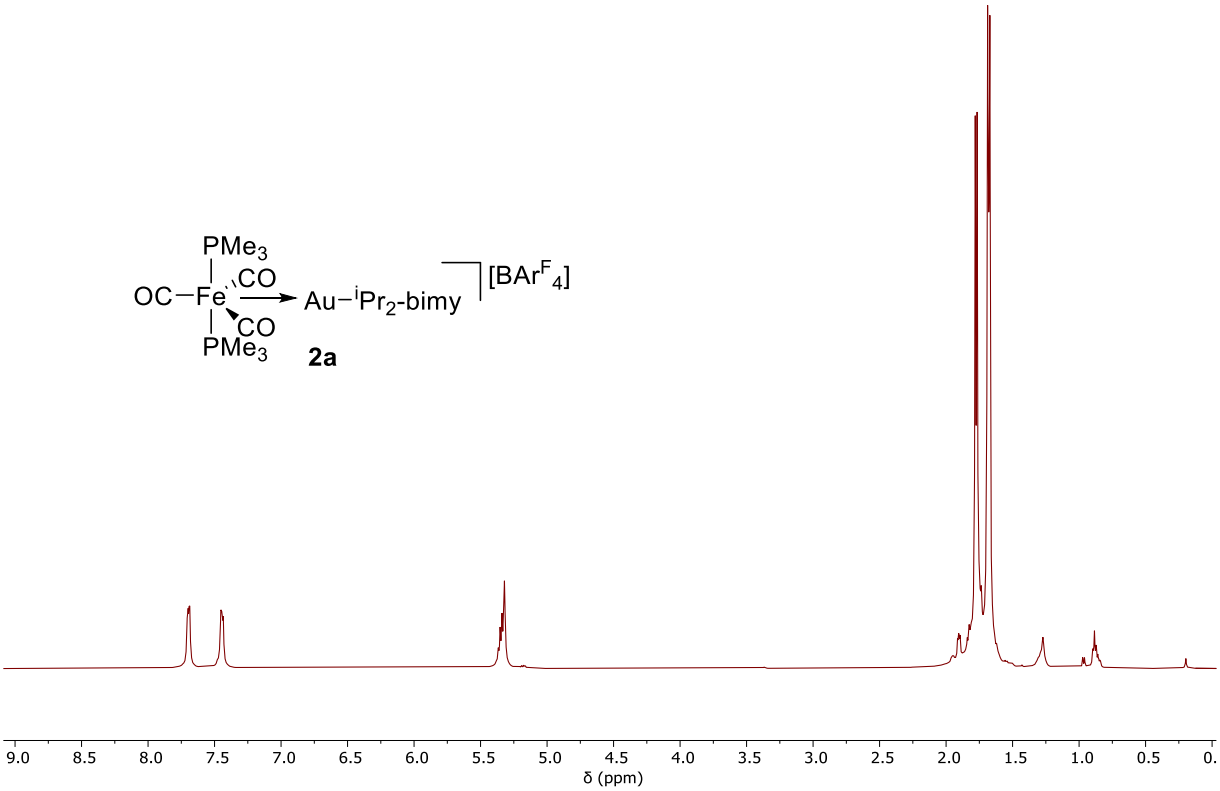

Figure S1. ^{1}H NMR spectrum of **2a** in CD_2Cl_2.

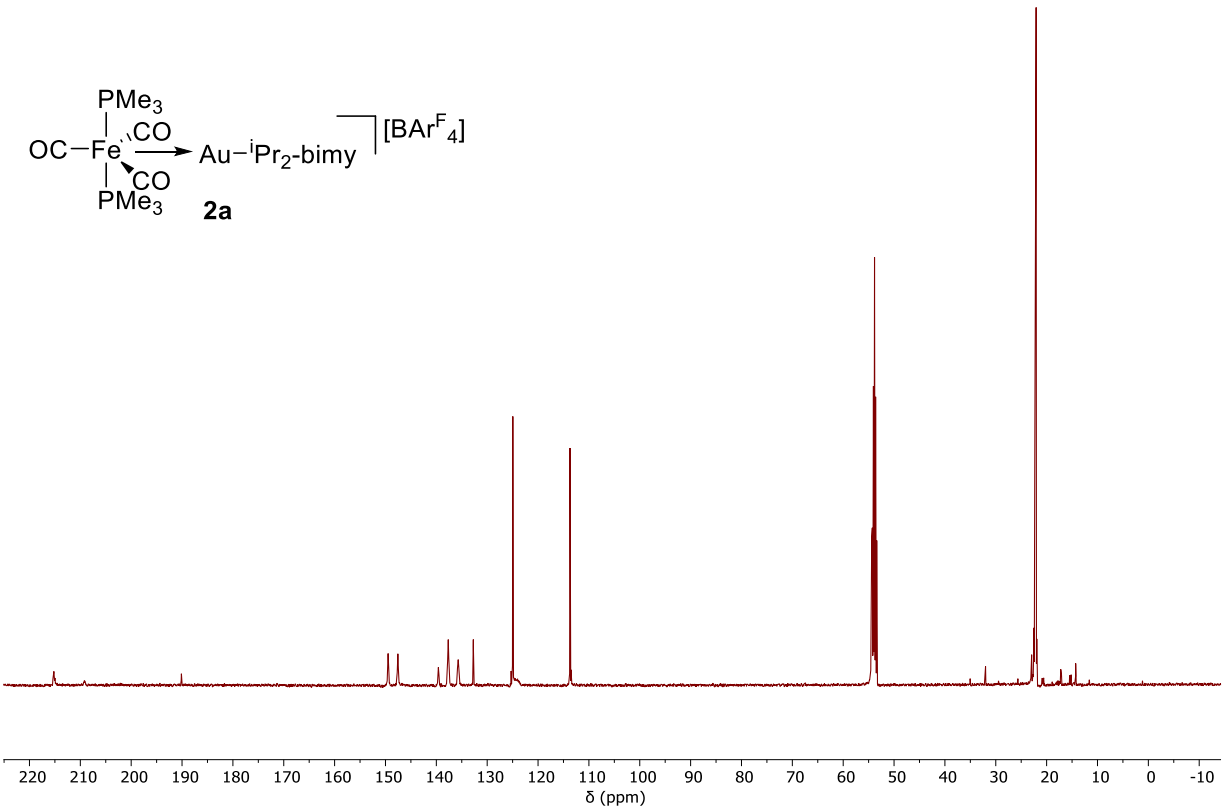

Figure S2a. $^{13}C\{^{1}H\}$ NMR spectrum of **2a** in CD_2Cl_2.

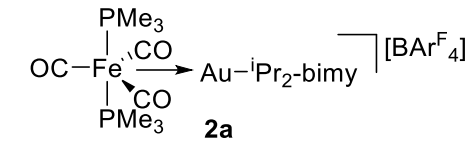

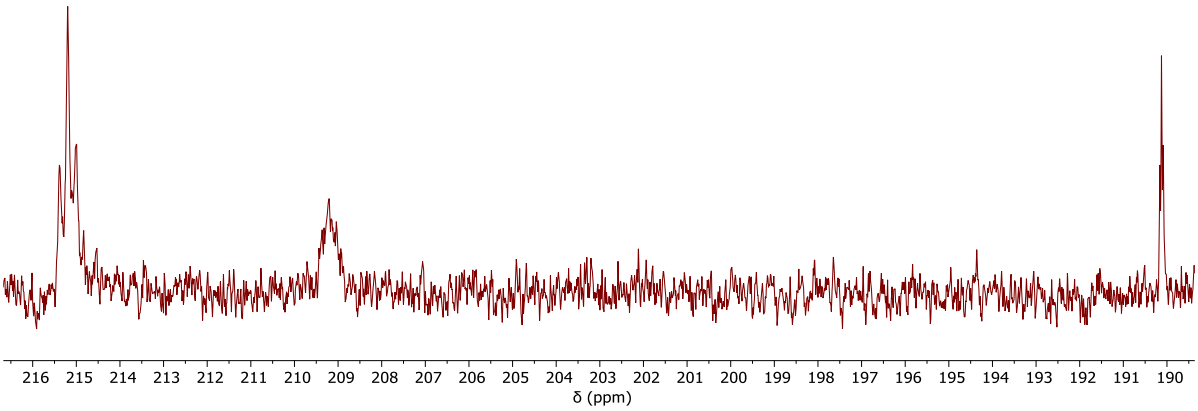

Figure S2b. Expansion of downfield section of $^{13}C\{^{1}H\}$ NMR spectrum of **2a** in CD_2Cl_2.

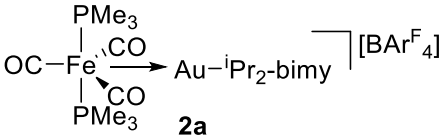

Figure S3. $^{31}P\{^{1}H\}$ NMR spectrum of **2a** in CD_2Cl_2. *[Au(**1a**)$_2$][BAr^F_4] formed from disproportionation.

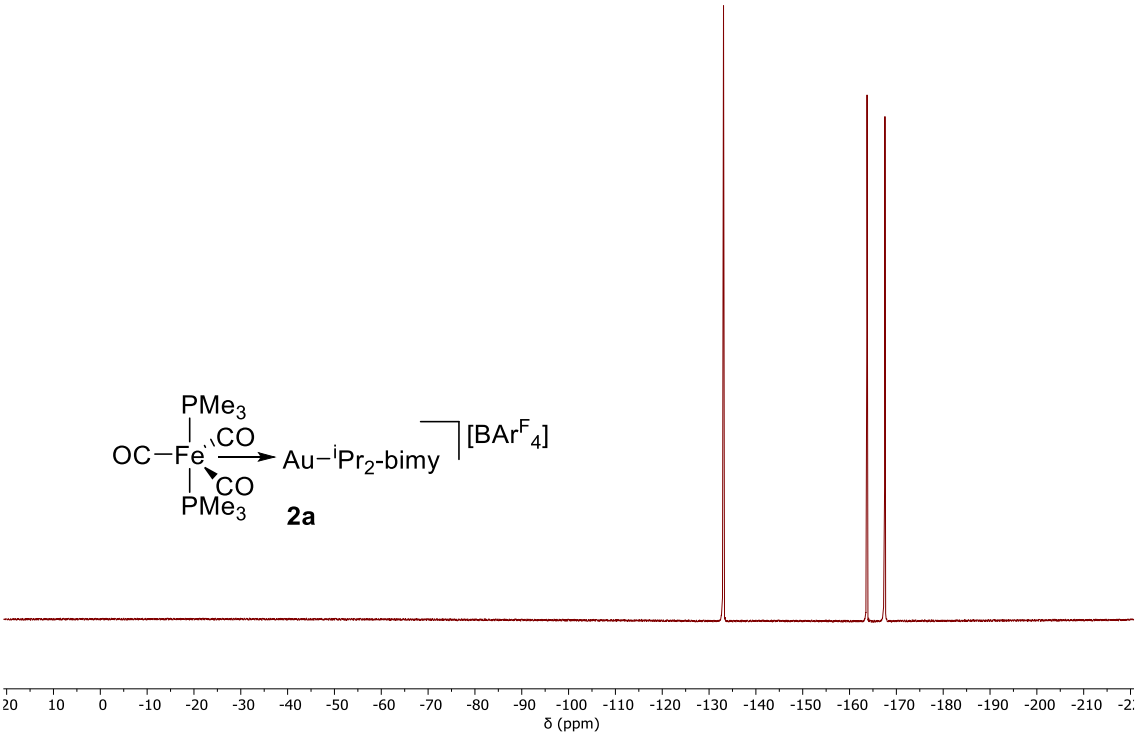

Figure S4. $^{19}F\{^{1}H\}$ NMR spectrum of **2a** in CD_2Cl_2.

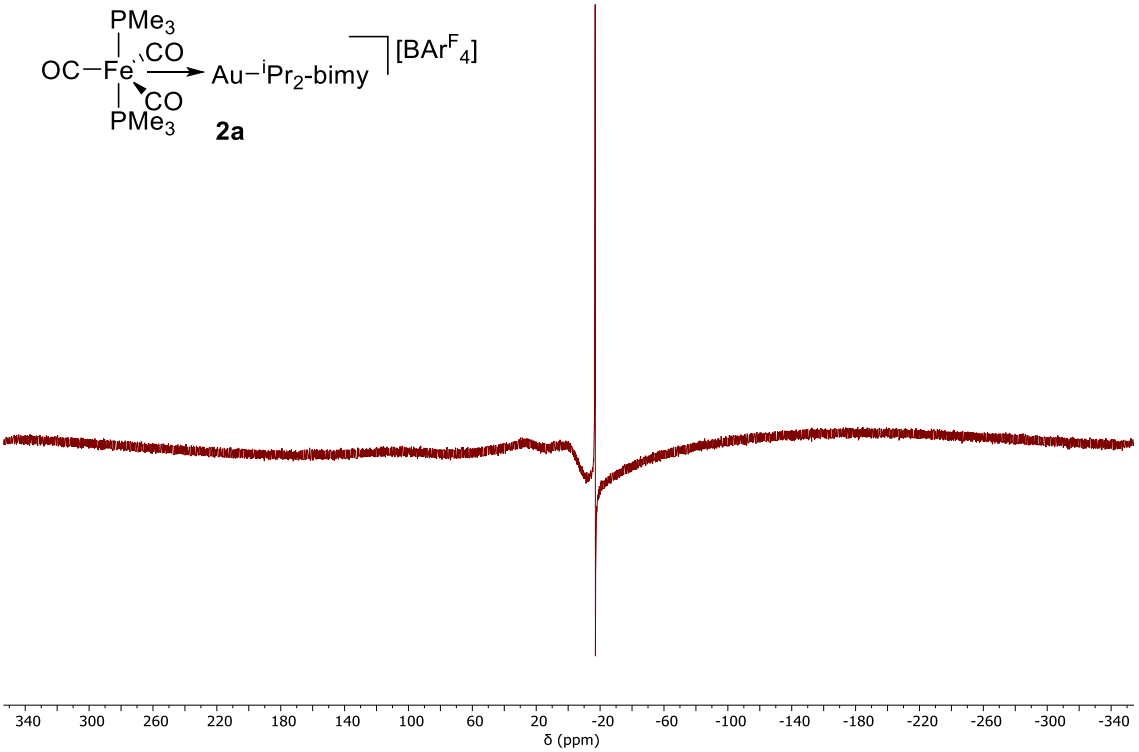

Figure S5. $^{11}B\{^{1}H\}$ NMR spectrum of **2a** in CD_2Cl_2.

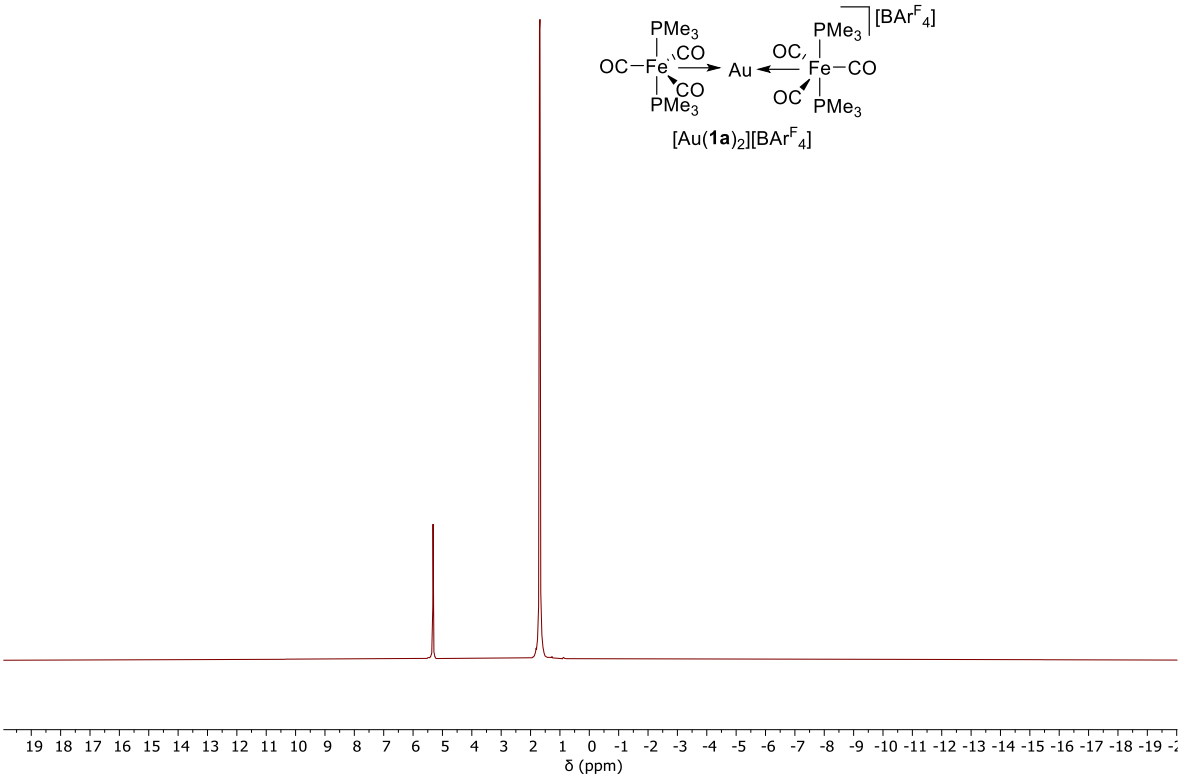

Figure S6. ^{1}H NMR spectrum of **[Au(1a)$_2$][BAr$^F_4$]** in CD_2Cl_2.

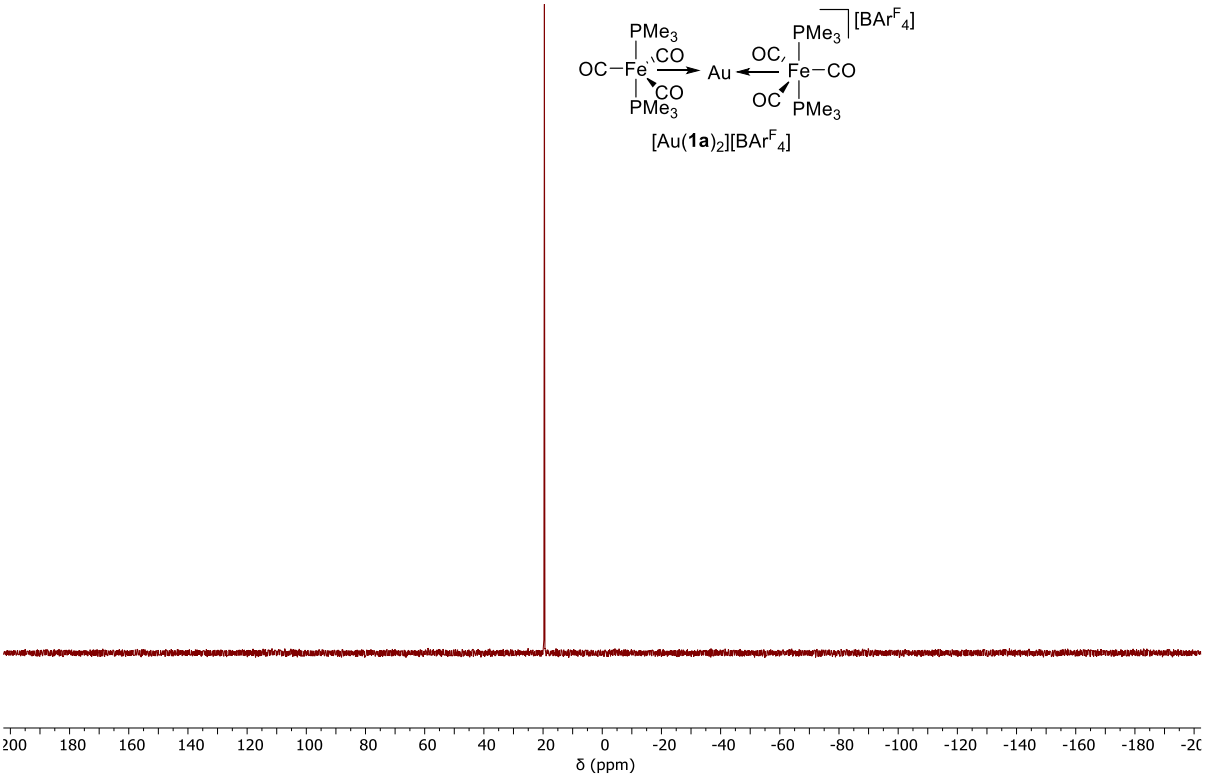

Figure S7. ^{31}P{^{1}H} NMR spectrum of **[Au(1a)$_2$][BAr$^F_4$]** in CD_2Cl_2.

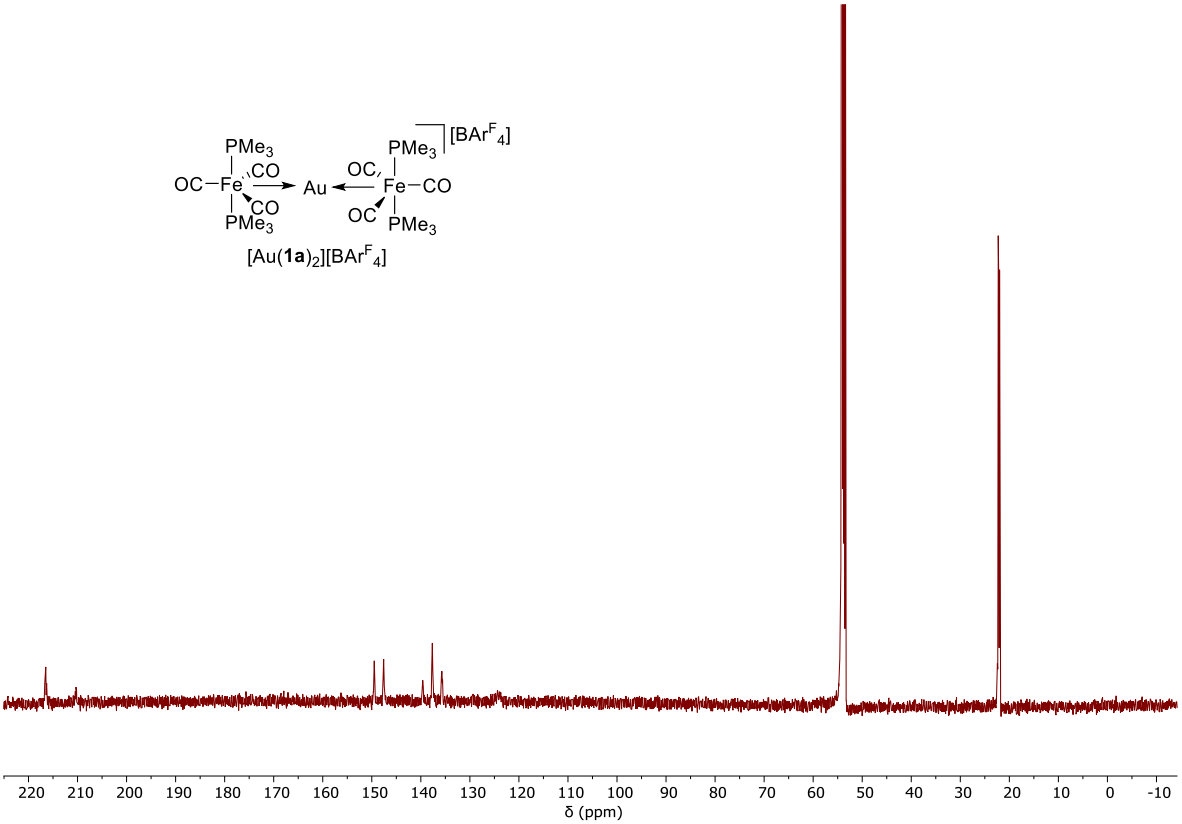

Figure S8. $^{13}C\{^{1}H\}$ NMR spectrum of **[Au(1a)$_2$][BAr$^F_4$]** in CD_2Cl_2.

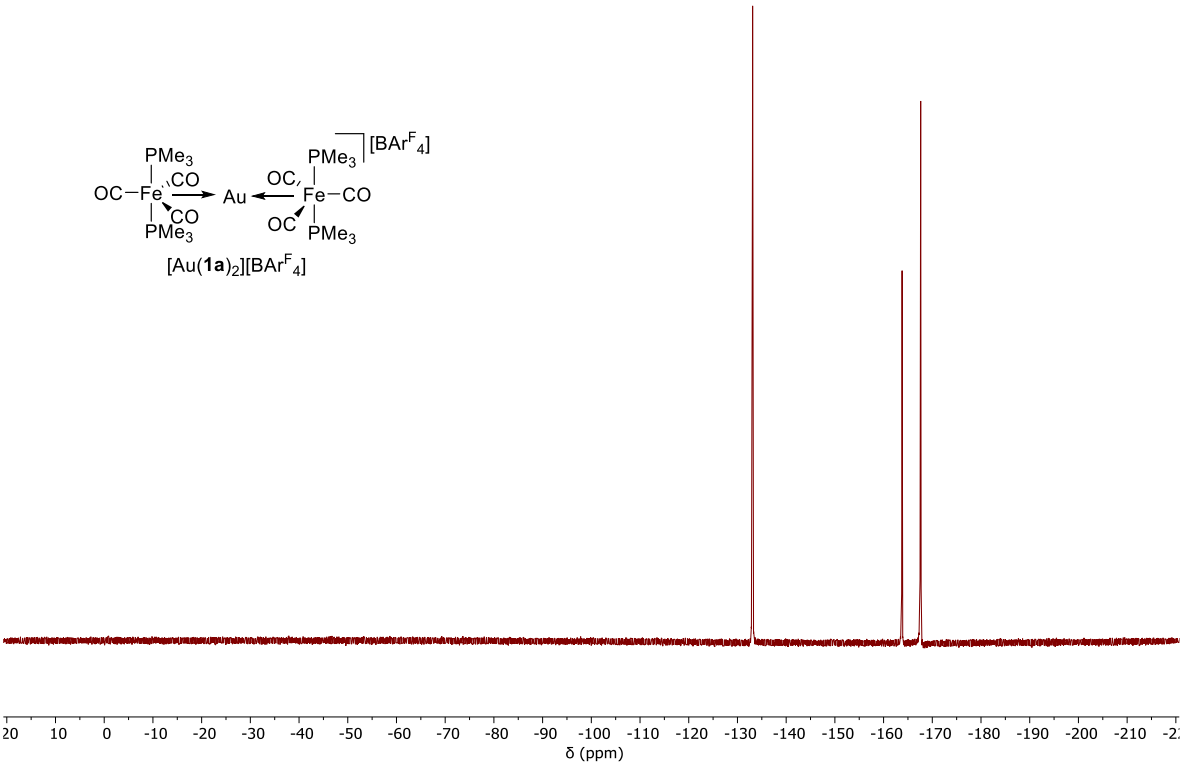

Figure S9. $^{19}F\{^{1}H\}$ NMR spectrum of **[Au(1a)$_2$][BAr$^F_4$]** in CD_2Cl_2.

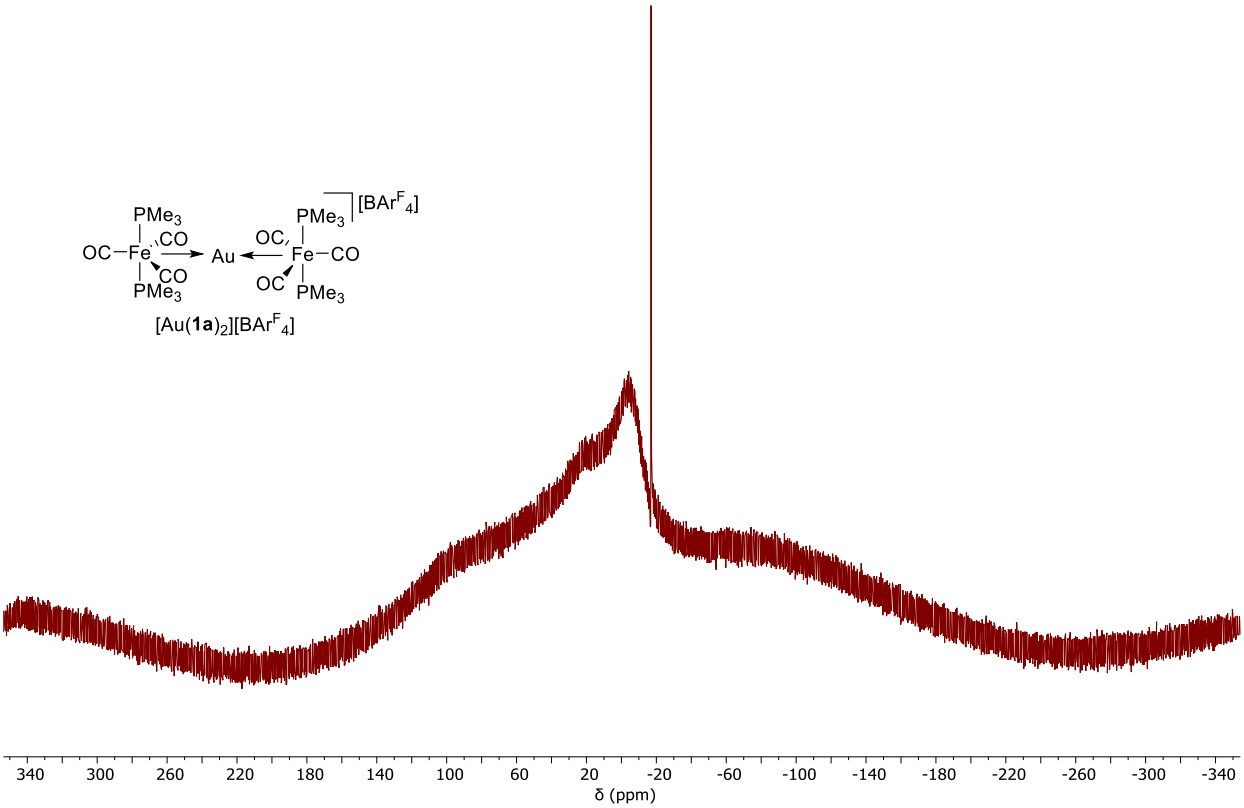

Figure S10. $^{11}B\{^{1}H\}$ NMR spectrum of **[Au(1a)$_2$][BAr$^F_4$]** in CD_2Cl_2.

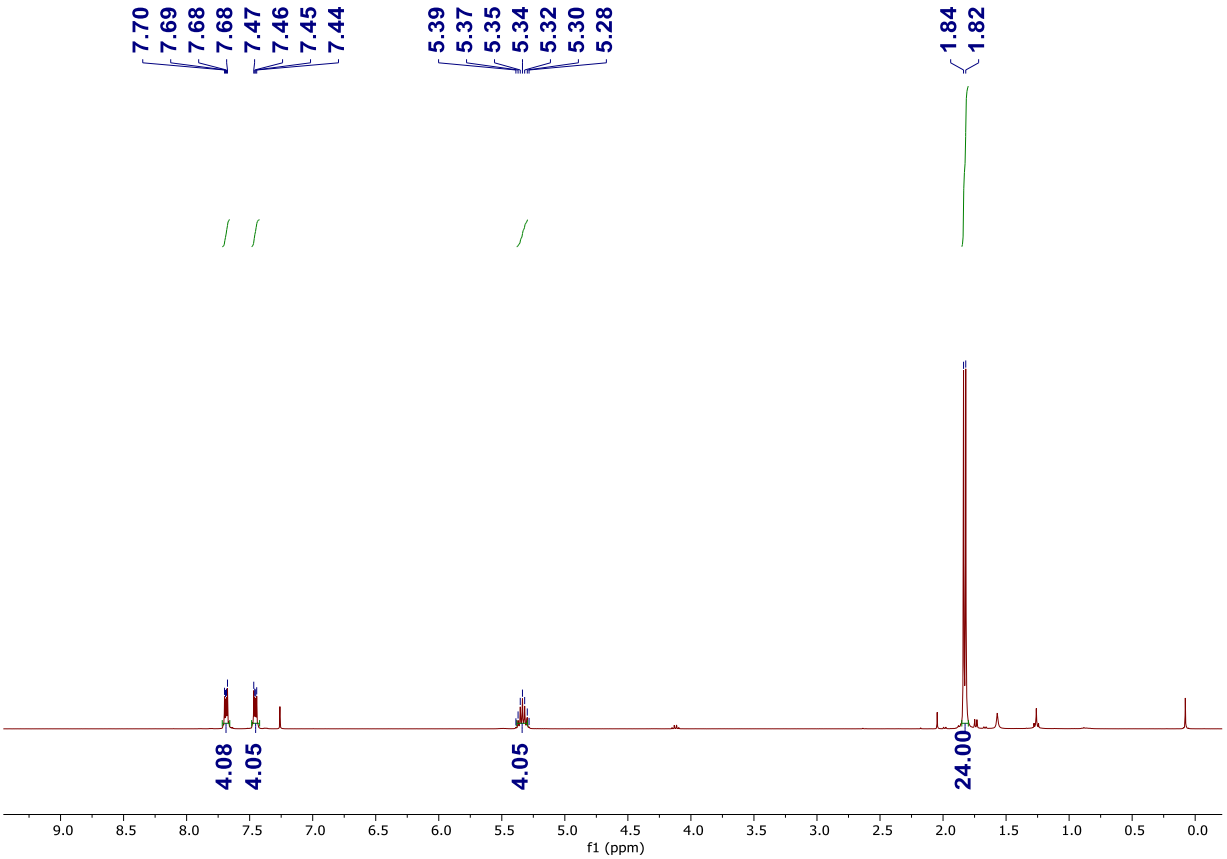

Figure S11. ^{1}H NMR spectrum of **[Au(^{i}Pr$_2$-bimy)$_2$][BAr$^F_4$]** in $CDCl_3$.

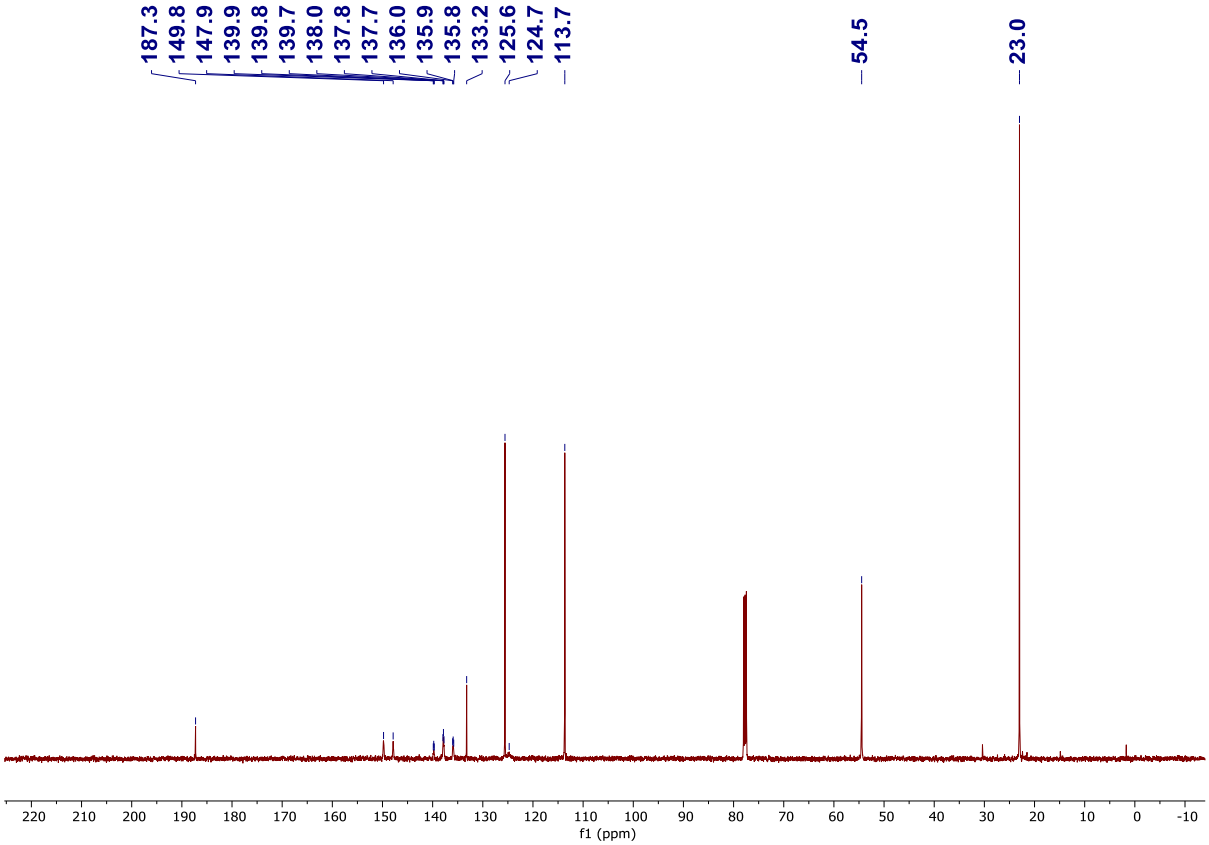

Figure S12. $^{13}C\{^{1}H\}$ NMR spectrum of **[Au(*i*Pr$_2$-bimy)$_2$][BAr$^F_4$]** in $CDCl_3$.

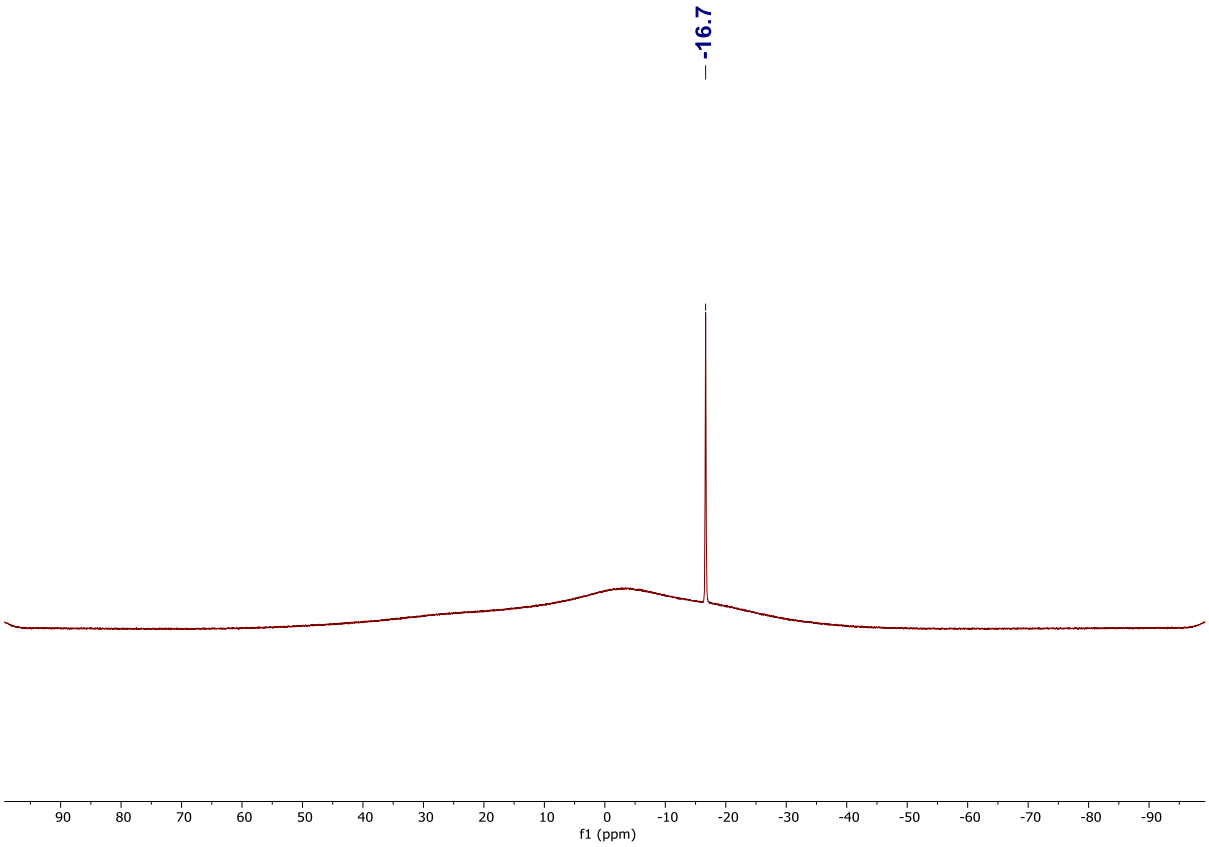

Figure S13. ^{11}B NMR spectrum of **[Au(*i*Pr$_2$-bimy)$_2$][BAr$^F_4$]** in $CDCl_3$.

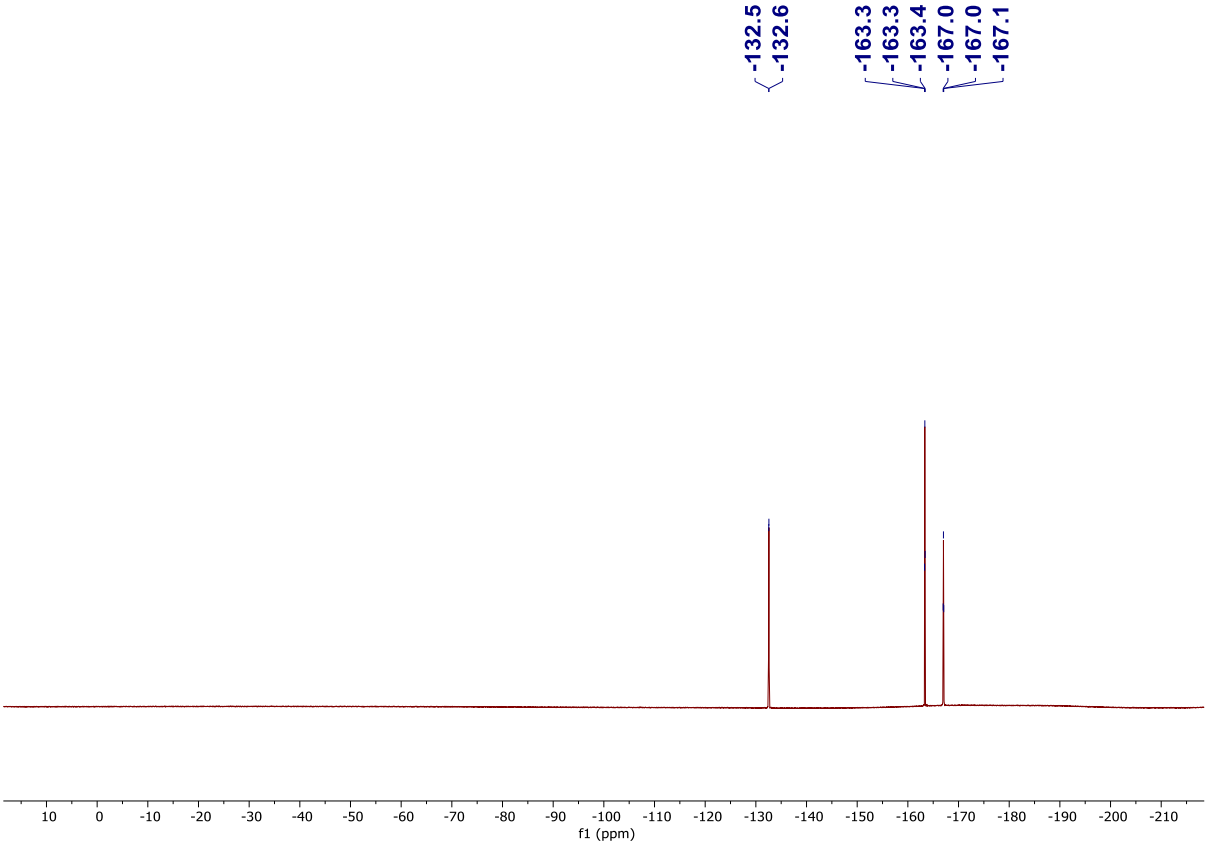

Figure S14. ^{19}F NMR spectrum of **[Au(*i*Pr$_2$-bimy)$_2$][BAr$^F_4$]** in $CDCl_3$.

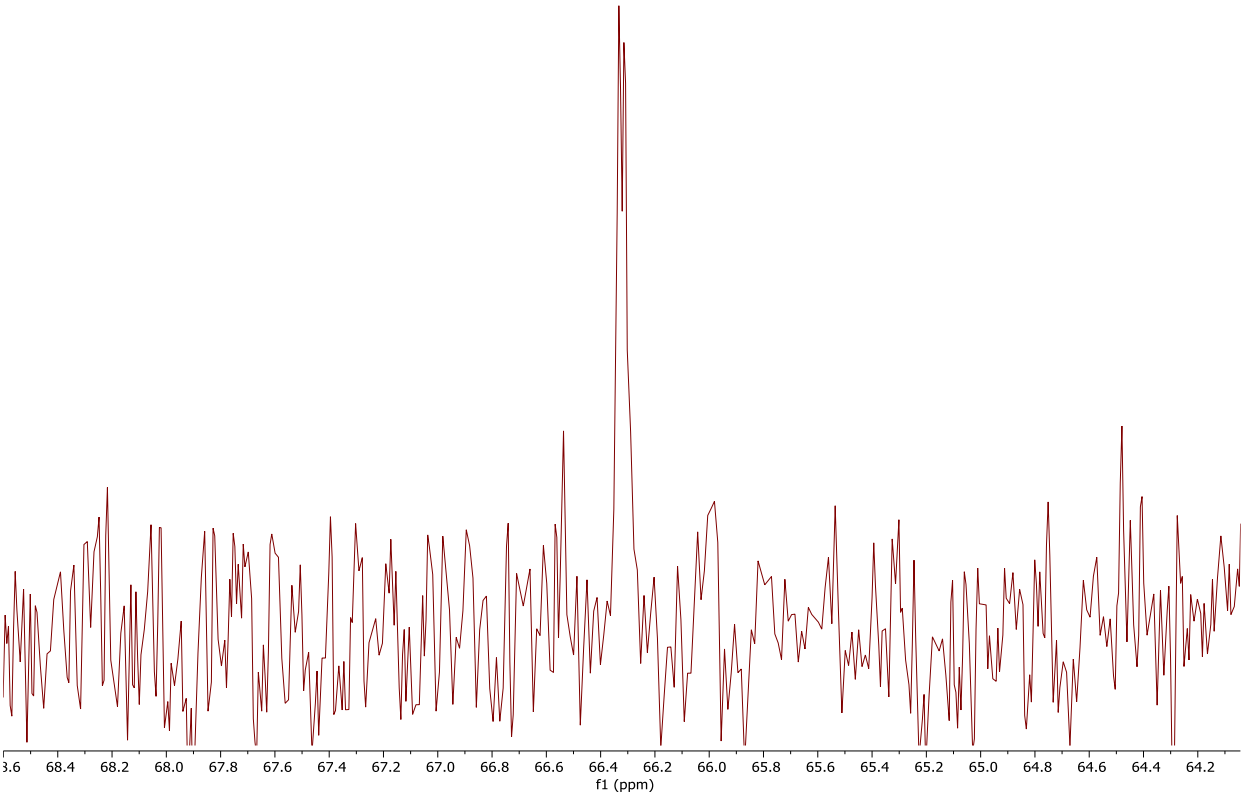

Figure S15. $^{31}P\{^1H\}$ NMR spectrum of [^{13}C]**2b** in CD_2Cl_2.

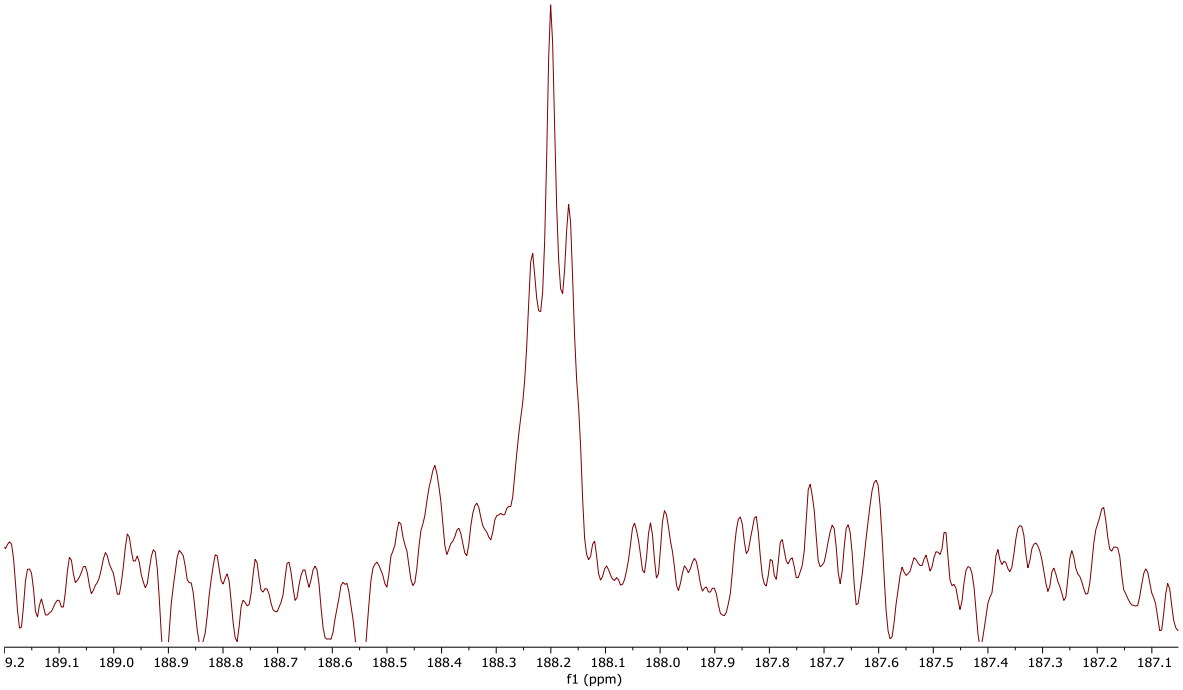

Figure 16. $^{13}C\{^{1}H\}$ NMR spectrum of [^{13}C]**2b** in CD_2Cl_2.

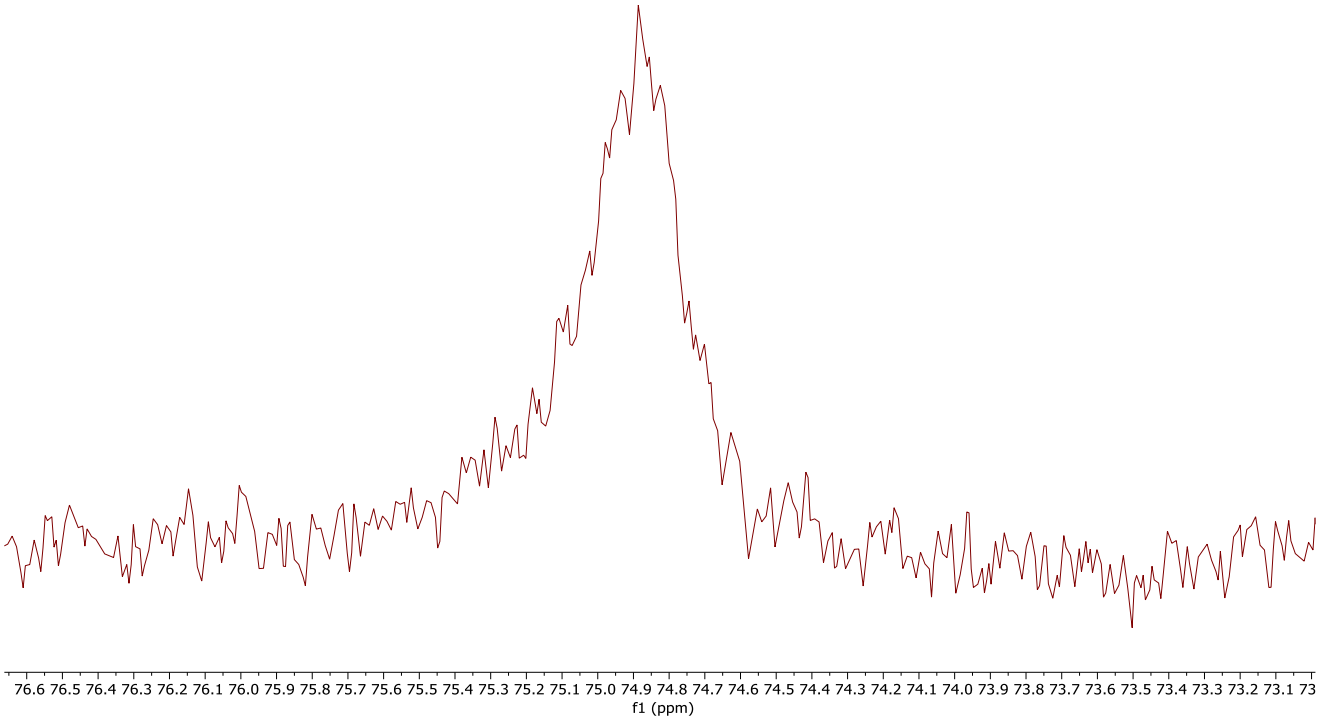

Figure S17. $^{31}P\{^{1}H\}$ NMR spectrum of [^{13}C]**2c** in CD_2Cl_2.

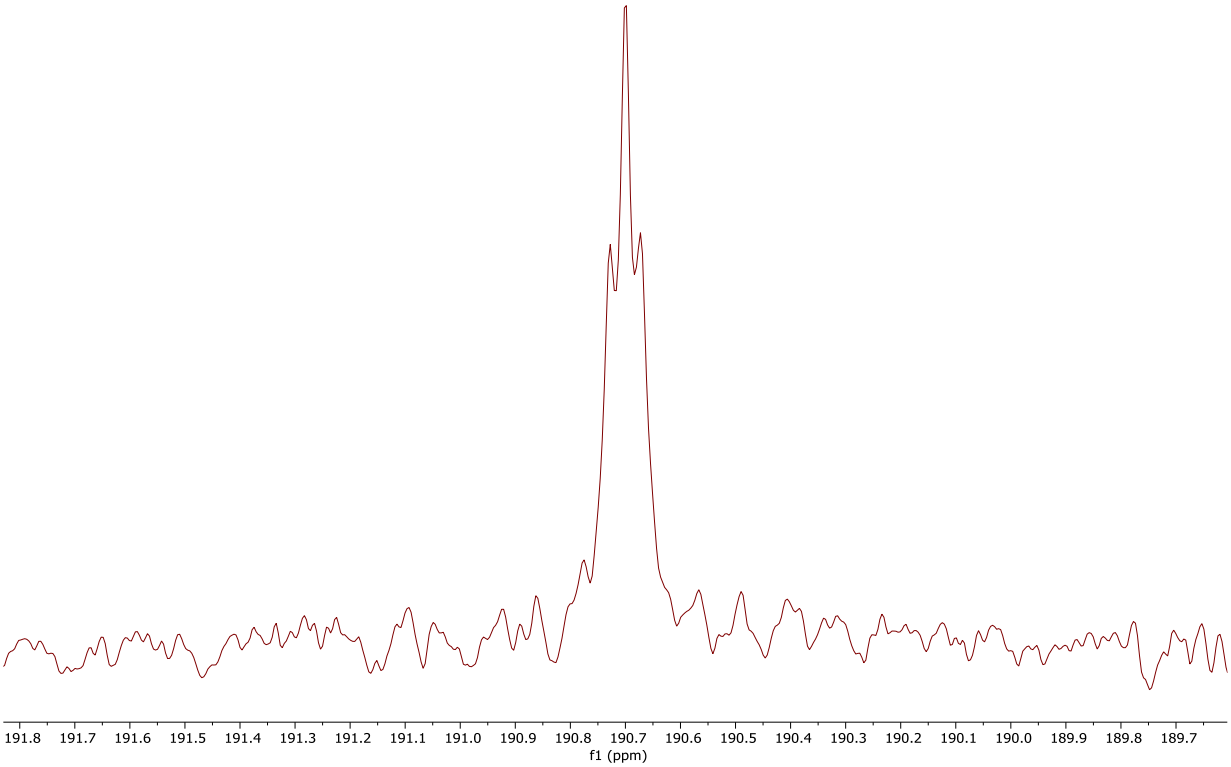

Figure 18. $^{13}C\{^{1}H\}$ NMR spectrum of [^{13}C]**2c** in CD_2Cl_2.

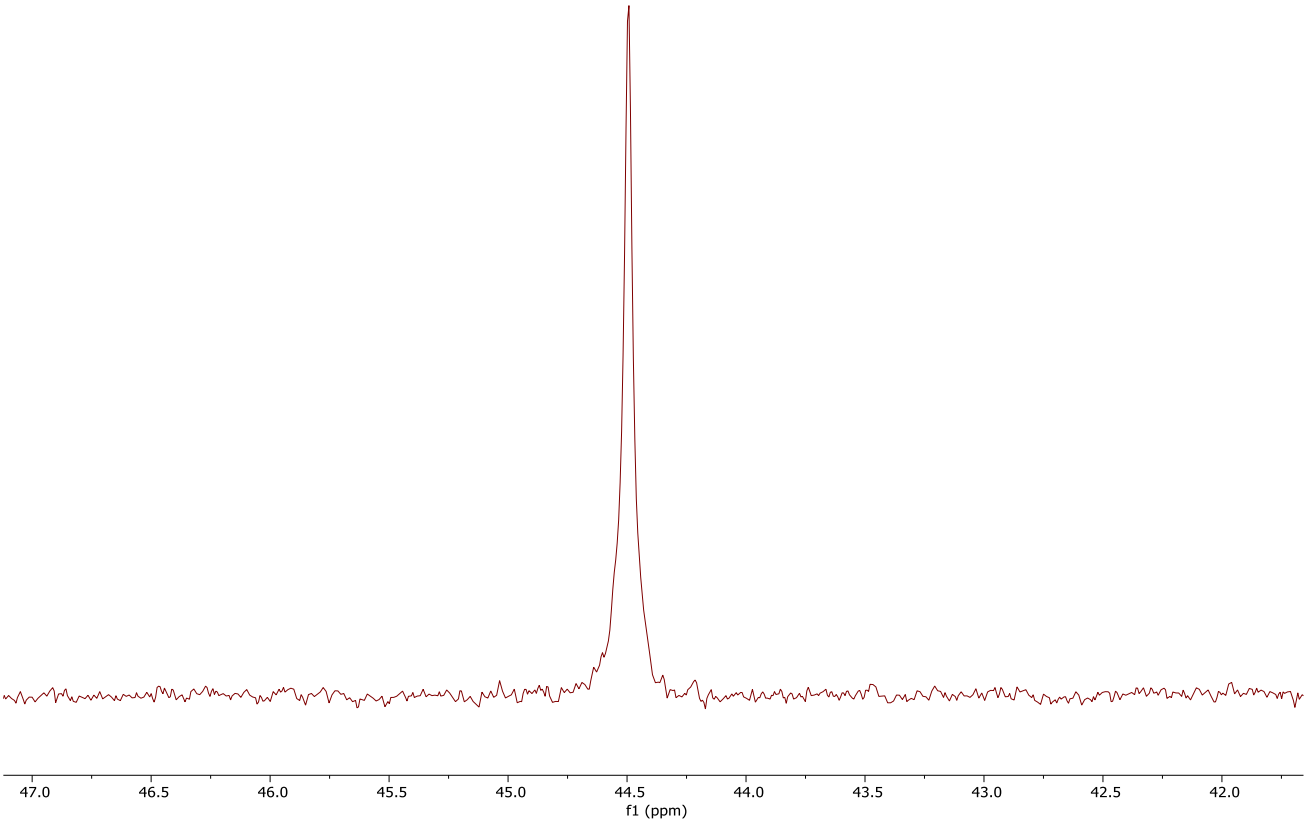

Figure S19. $^{31}P\{^{1}H\}$ NMR spectrum of **2d** in CD_2Cl_2.

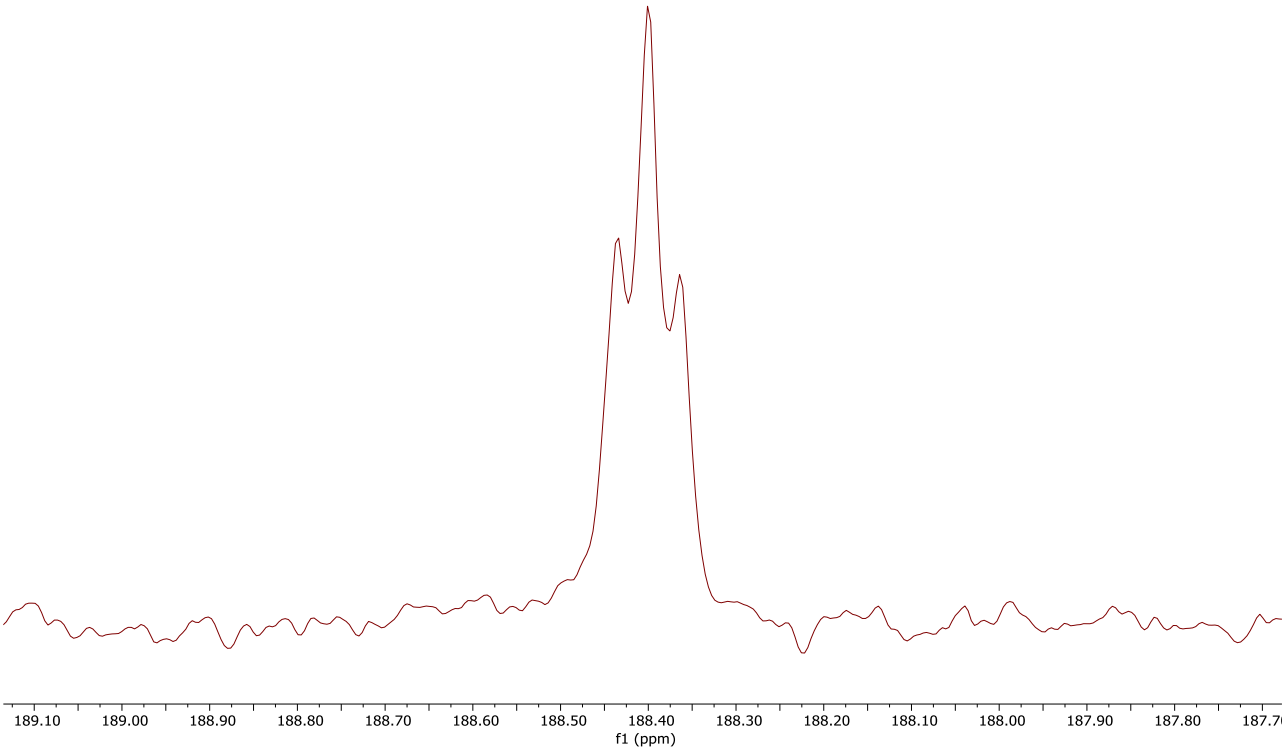

Figure 20. $^{13}C\{^{1}H\}$ NMR spectrum of **2d** in CD_2Cl_2.

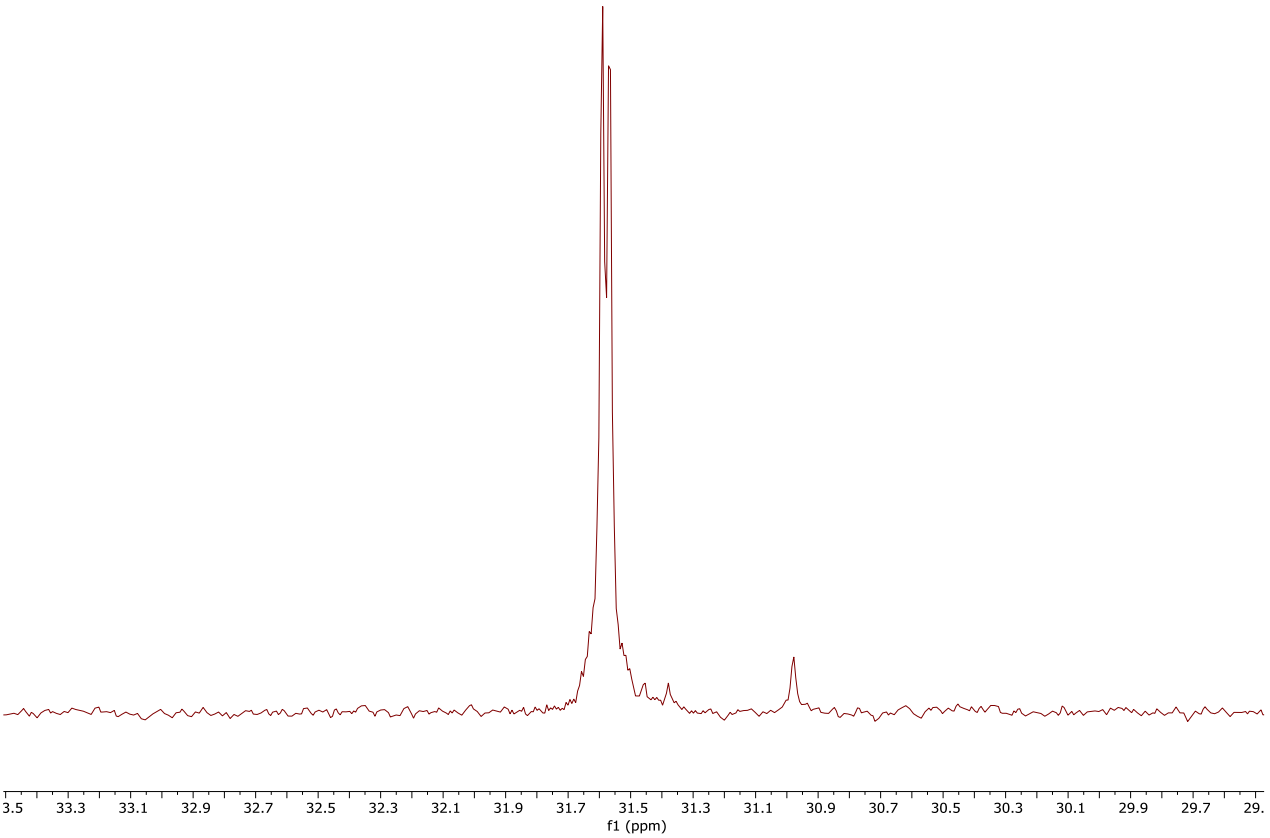

Figure S21. $^{31}P\{^{1}H\}$ NMR spectrum of [^{13}C]**2e** in CD_2Cl_2.

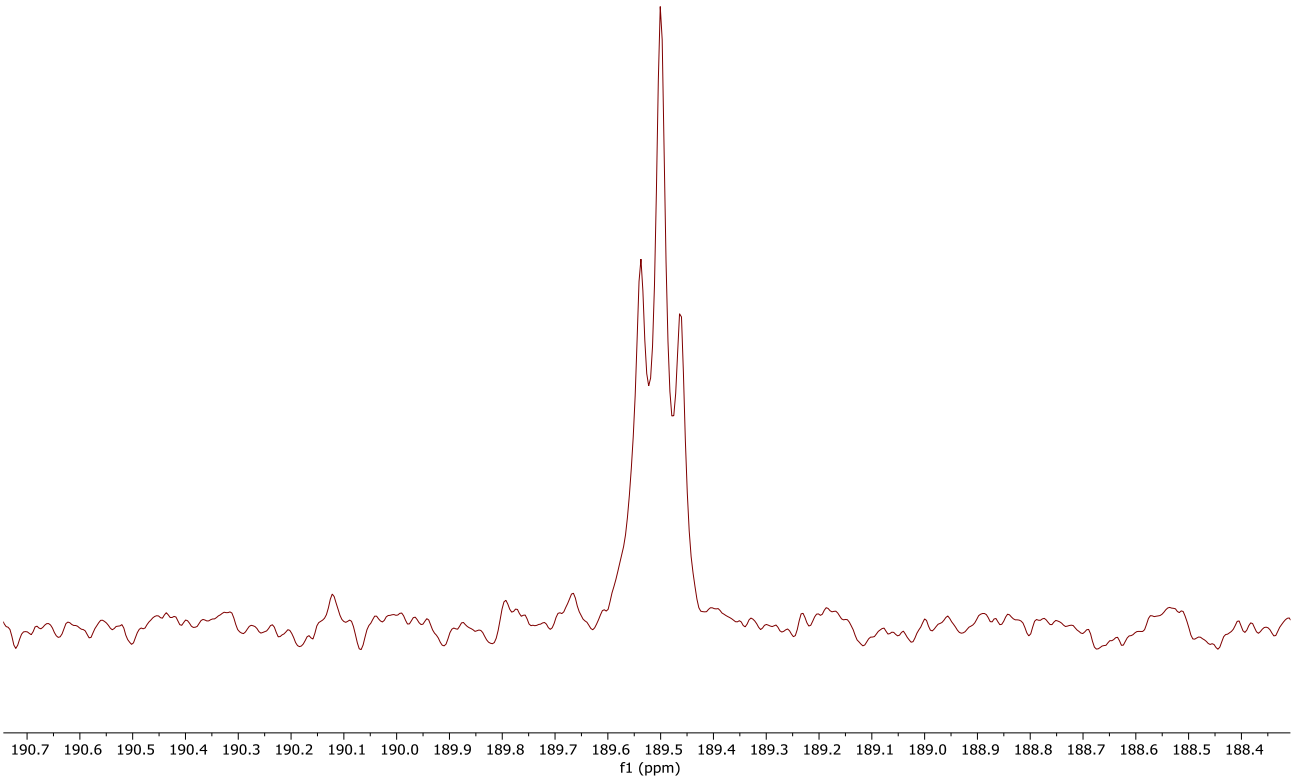

Figure 22. $^{13}C\{^{1}H\}$ NMR spectrum of [^{13}C]**2e** in CD_2Cl_2.

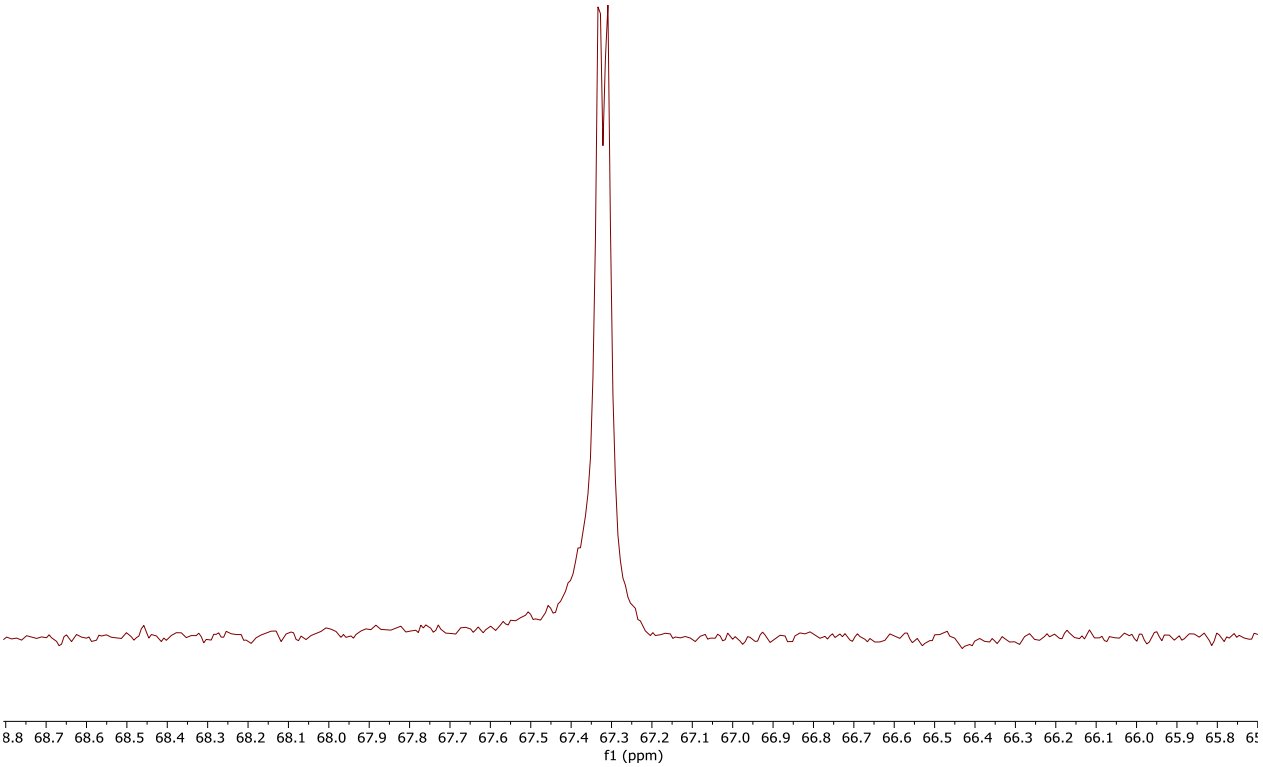

Figure S23. $^{31}P\{^{1}H\}$ NMR spectrum of [^{13}C]**2f** in CD_2Cl_2.

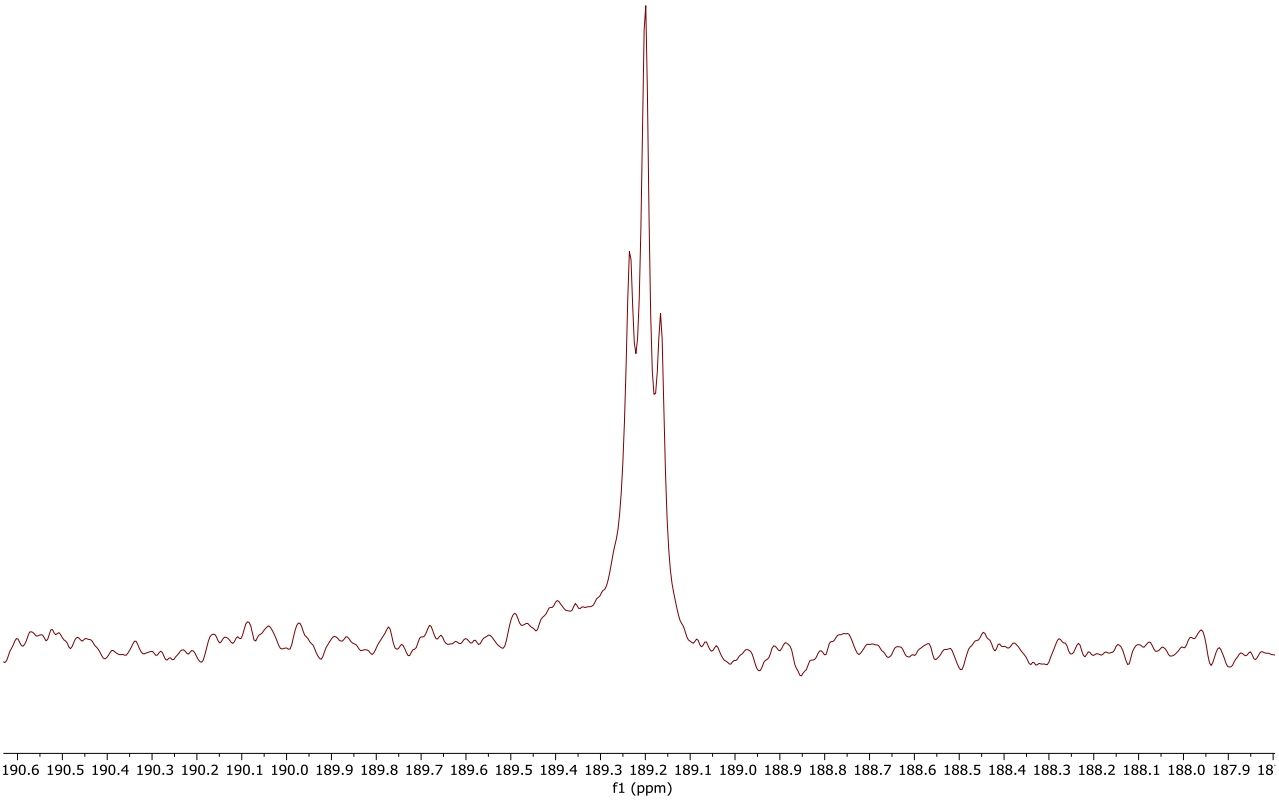

Figure 24. $^{13}C\{^{1}H\}$ NMR spectrum of [^{13}C]**2f** in CD_2Cl_2.

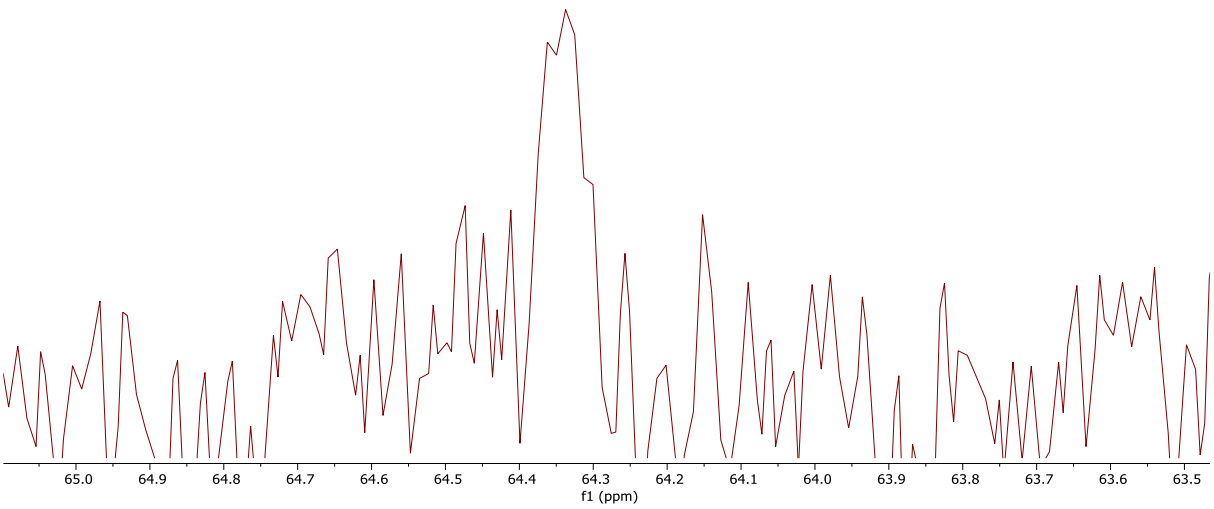

Figure S25. $^{31}P\{^{1}H\}$ NMR spectrum of [^{13}C]**2g** in CD_2Cl_2.

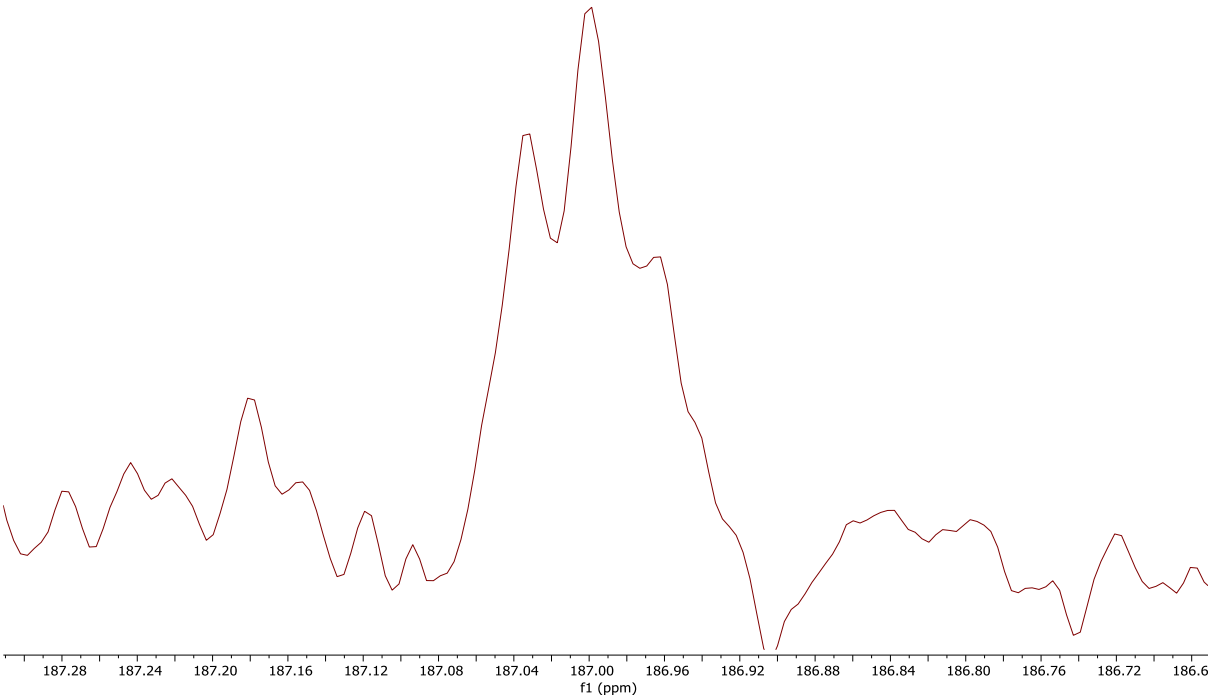

Figure 26. $^{13}C\{^{1}H\}$ NMR spectrum of [^{13}C]**2g** in CD_2Cl_2.

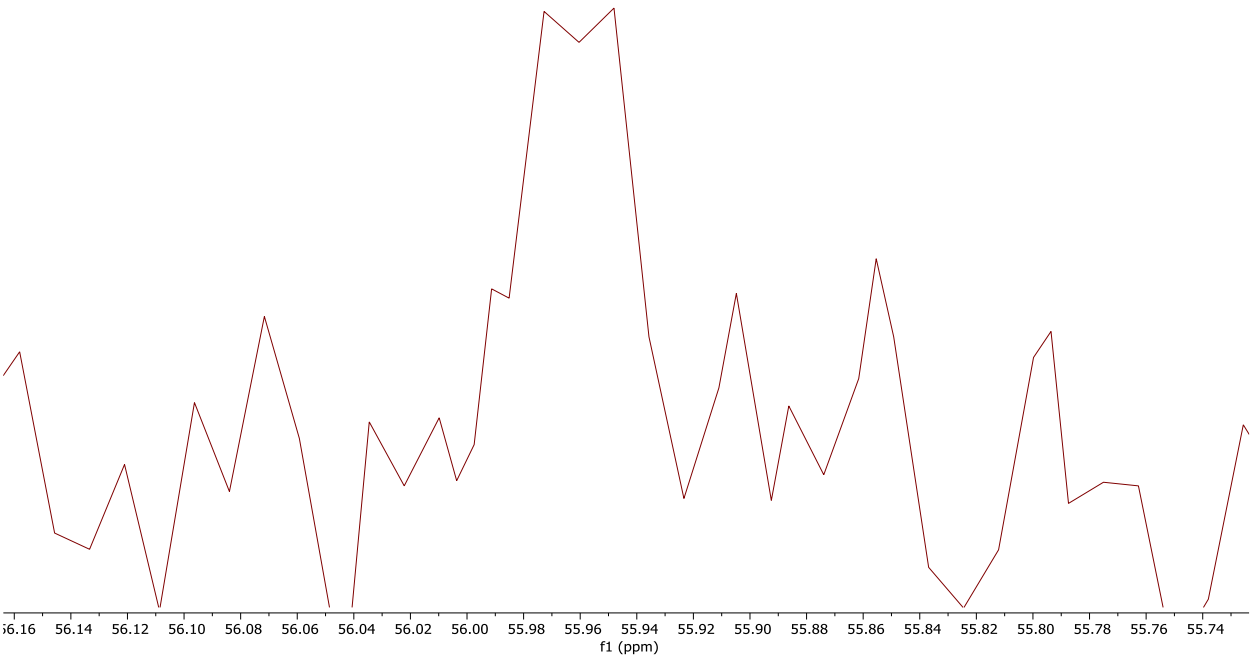

Figure S27. $^{31}P\{^{1}H\}$ NMR spectrum of [^{13}C]**2h** in CD_2Cl_2.

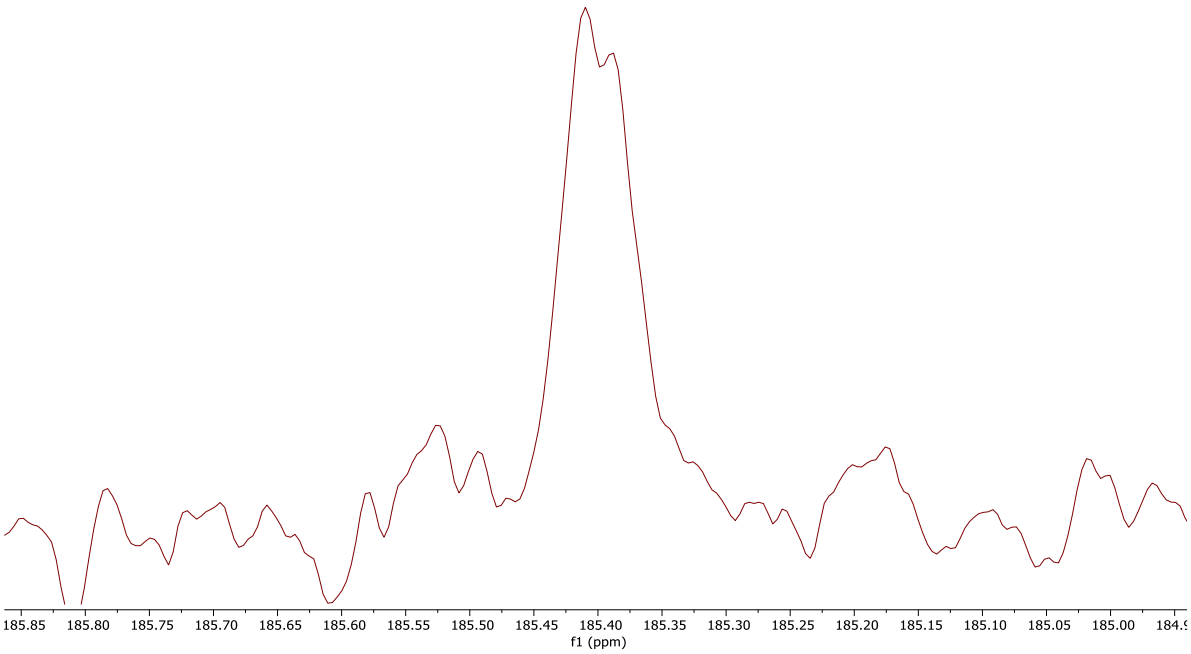

Figure 28. $^{13}C\{^{1}H\}$ NMR spectrum of [^{13}C]**2h** in CD_2Cl_2.

Mass Spectra

Meas. m/z	#	Formula	Calc. Mass	Err [ppm]
689.1255	1	C22 H36 Au Fe N2 O3 P2	689.1257	0.29

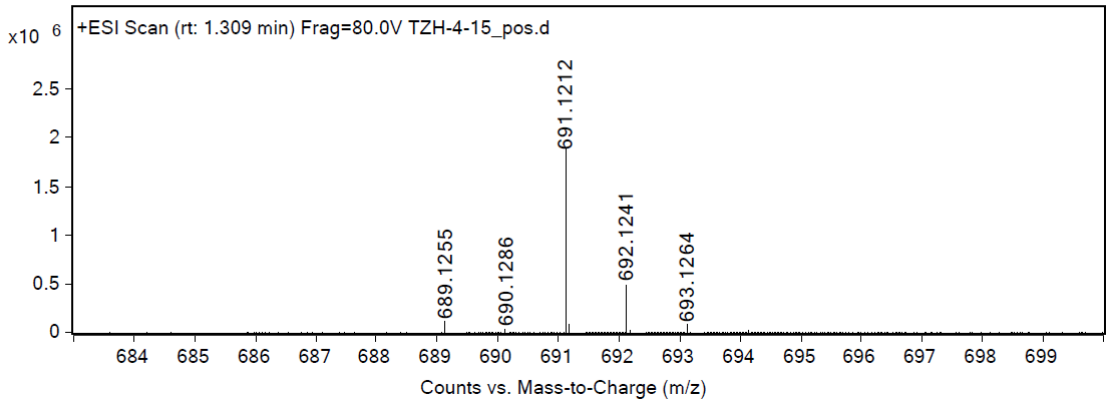

Figure S29. Positive mode HR-ESI-MS spectrum of **2a**.

Meas. m/z	#	Formula	Calc. Mass	Err [ppm]
677.9784	1	C24 B F20	677.9783	0.15

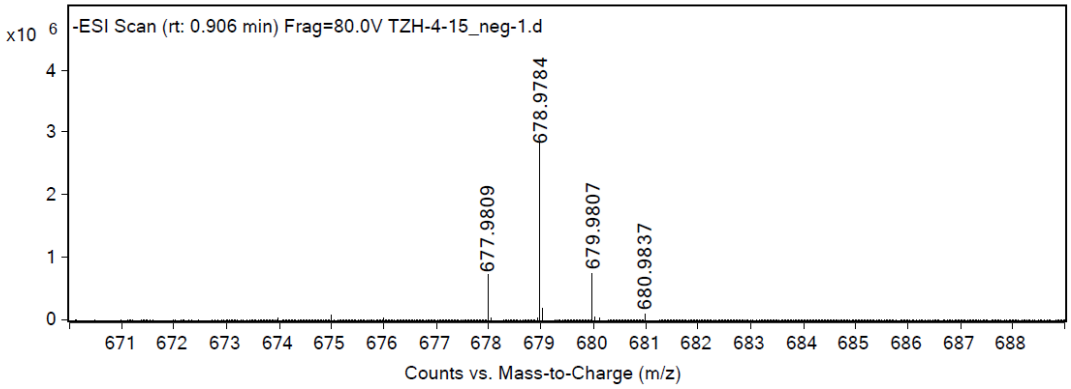

Figure S30. Negative mode HR-ESI-MS spectrum of **2a**.

Meas. m/z	#	Formula	Calc. Mass	Err [ppm]
780.9824	1	C18 H36 Au Fe2 O6 P4	780.9821	0.38

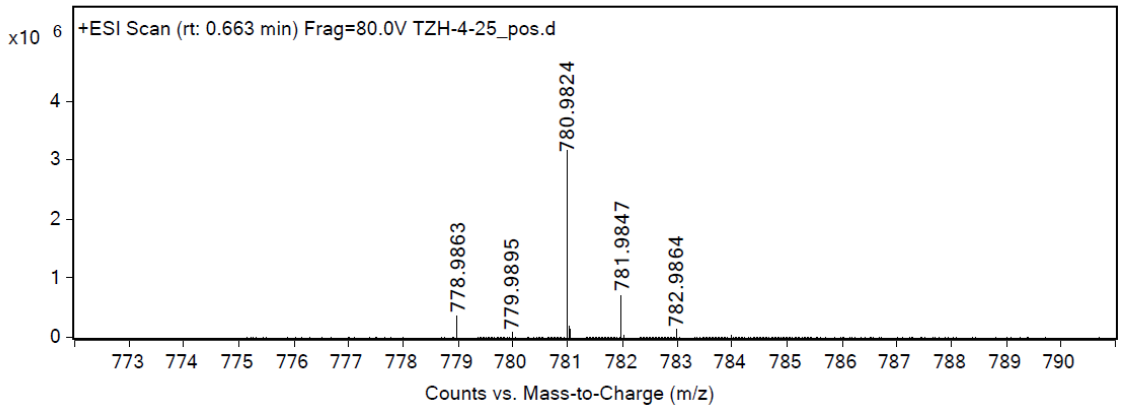

Figure S31. Positive mode HR-ESI-MS spectrum of **[Au(1a)$_2$][BAr$^F{}_4$]**.

Meas. m/z	#	Formula	Calc. Mass	Err [ppm]
678.9779	1	C24 B F20	678.9783	0.59

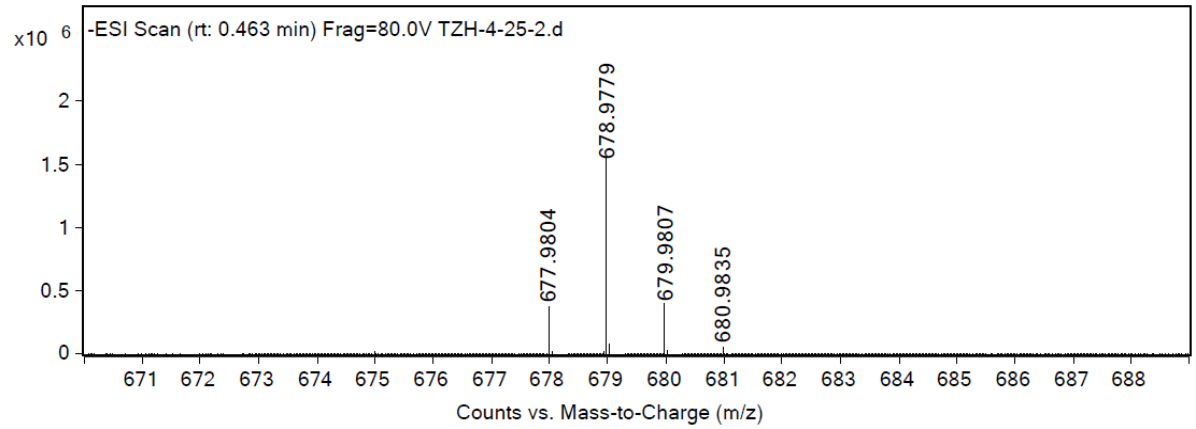

Figure S32. Negative mode HR-ESI-MS spectrum of **[Au(1a)$_2$][BAr$^F{}_4$]**.

X-Ray Crystallography Data

Data	2a	$[Au(1a)_2][BAr^F_4]$
Formula	$C_{46}H_{36}AuBF_{20}FeN_2O_3P_2$	$C_{42}H_{36}AuBF_{20}Fe_2O_6P_4$
Formula weight	1370.33	1460.06
Colour/shape	Colourless block	Colourless needle
Crystal size / mm^3	0.08 × 0.11 × 0.17	0.06 x 0.08 x 0.46
Temperature / K	100	100
Crystal system	Monoclinic	Monoclinic
Space group	P 21/c	P 2/n
***a* / Å**	15.5530(13)	16.0840(7)
***b* / Å**	20.5519(13)	8.3385(3)
***c* / Å**	16.8582(10)	19.9778(9)
α / °	90	90
β / °	116.003(3)	109.682(2)
γ / °	90	90
***V* / Å^3**	4843.1(6)	2522.81(18)
Z	4	2
ρ_{calcd} / g cm^{-3}	1.879	1.922
Radiation used	Mo-Kα	Mo-Kα
μ / mm^{-1}	3.513	3.715
***2θ max* / °**	57.4	52.75
No. of unique reflns	12477	5151
No. of variables	695	350
GoF (S)	1.035	1.033
R factor (I > 2σ)	0.0292 (10249 reflections)	0.0161 (5064 reflections)

Table S1. Crystal Data, Data Collection and Refinement Parameters for the structure of **2a** (CCDC 2206892) and **$[Au(1a)_2][BAr^F_4]$** (CCDC 2206893).

DFT Calculations

Computational Methods

Unconstrained geometry optimisations and subsequent frequency calculations of all species were performed with the BP86 GGA functional.[3] The Karlsruhe def2-TZVP basis set was employed on Au, Fe, N, P and C(NHC) atoms as well as the CO ligands.[4] For the element Au the basis set is paired with the def2 scalar relativistic effective core potential.[5] The smaller def2-SVP basis set was used on the remaining atoms.[6] Dispersion effects were incorporated using Grimme's D3 parameter set along with Becke-Johnson damping.[7] These calculations were carried out with the Gaussian 16 (Revision B.01) program.[8] Initial coordinates were extracted from the experimental single-crystal structure. The absence of imaginary eigenvalues of the Hessian confirmed the presence of true minima for all optimised geometries. Natural bond orbital (NBO) analysis[8] was performed to evaluate the Wiberg Bond Indices using the NBO 6.0 program.[10] The Quantum theory of atoms in molecules analysis[11] was performed with the AIMALL program[12] using a wavefunction generated at the BP86-D3(BJ)/def2TZVPP/x2C-TZVPall level of theory, where the all-electron x2C-TZVPall basis set was used for Au atoms.[13] The bonding situation was further scrutinized by means of an local energy decomposition analysis (LED)[14] in conjunction with the natural orbitals for chemical valence (NOCV) method,[15] as implemented in the ORCA 5.0.2 program package.[16] The NOCV eigenvalues are computed alongside with the corresponding energy contributions obtained from the Extended Transition State (ETS) method developed by Ziegler. For the ETS-NOCV analysis single point calculations at the B3LYP-D3(BJ)/def2-TZVPP(+RECP on Au) level of theory were performed on the previously BP86-D3(BJ)-optimised geometries.[17] To accelerate the DFT calculations, the resolution of identity (RIJ) and chain-of-spheres approximations (COSX) were employed, [18] supplemented by the universal def2/J Coulomb fitting basis set.[19] For the LED analysis, closed-shell single point DLPNO-CCSD(T) calculations were performed using TightPNO settings.[20] The def2-TZVPP basis set was used in the conjunction with the matching def2-TZVPP/C auxiliary basis set. The RIJCOSX approximation was used for calculation of Coulomb and exchange integrals in the HF reference. The def2/J auxiliary basis was used. The Foster-Boys scheme was applied for localising PNOs in the LED scheme.[21] "VerytightSCF" convergence criteria were applied in all ORCA calculations. Binding energies (**Δ*E***) were calculated as the electronic energy difference between complex **2a** and its constituent fragments $\{Au(NHC^{iPr})\}^+$ and $\{Fe(CO)_3(PMe_3)_2\}$ at their equilibrium BP86-D3 geometries.

Bond parameters

Table S2. Comparison of key calculated and experimental bond parameters (Å, °) at the BP86-D3/def2-TZVP/def-SVP level along with Wiberg Bond Orders (WBI). Vibrational frequencies for CO stretching modes are also provided.

	DFT	WBI	Exp.
Au–Fe	2.587	0.06	2.562
Au–C(NHC)	2.030	0.39	2.032
Au–C(CO)	2.638	0.09	2.686
Au–C(CO)	2.649	0.09	2.533
Fe–P	2.262	0.42	2.236
Fe–P	2.242	0.42	2.246
Fe–CO	1.784	0.71	1.794
Fe–CO	1.783	0.71	1.785
Fe–CO	1.770	0.65	1.779
C–O	1.166	1.98	
C–O	1.161	2.07	
C–Fe–C	143.0	–	142.0
C–Fe–C	108.3	–	110.1
C–Fe–C	108.5	–	107.7
C(NHC)–Au–C	140.1	–	142.0
C(NHC)–Au–C	140.3	–	137.1
P–Fe–P	178.2	–	176.9
v(CO) [cm^{-1}]	1919, 1945, 1993	–	

Quantum Theory of Atoms in Molecules (QTAIM) Analysis

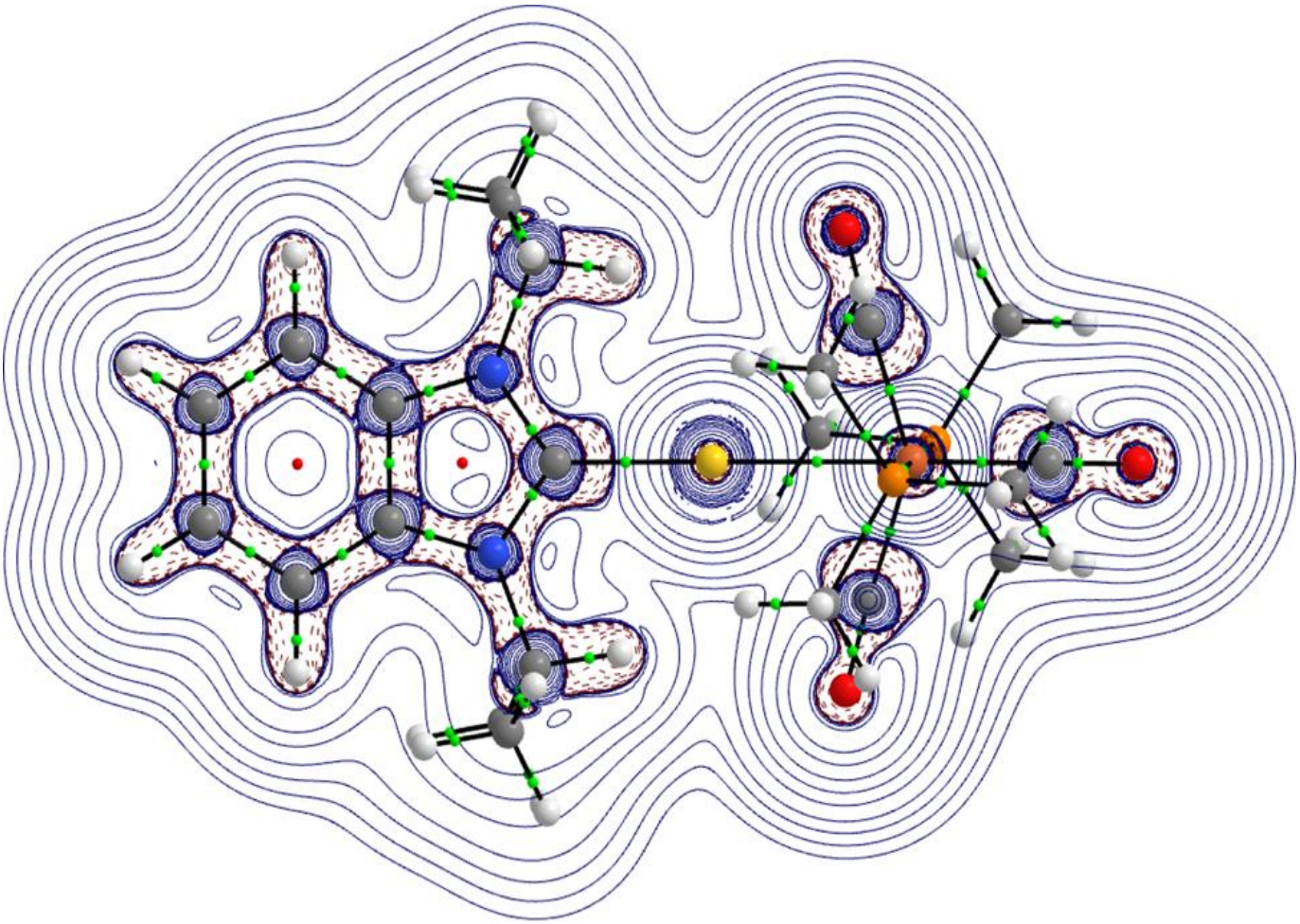

Figure S33. Contour plot of the Laplacian of electron density $\nabla^2\rho(r)$ in the Au-Fe-$C_{(CO)}$ plane of [Au(NHC)Fe$(CO)_3(PMe_3)_2$] at the BP86-D3(BJ)/def2TZVPP/x2C-TZVPall level. Values of key topological descriptors are also given. Blue solid lines indicate regions of charge depletion ($\nabla^2\rho(r)>0$) and red dotted lines indicate regions of charge accumulation ($\nabla^2\rho(r)<0$). Green and red dots represent bond and ring critical points, respectively.

Natural Orbitals for Chemical Valence / Extended Transition State Analysis

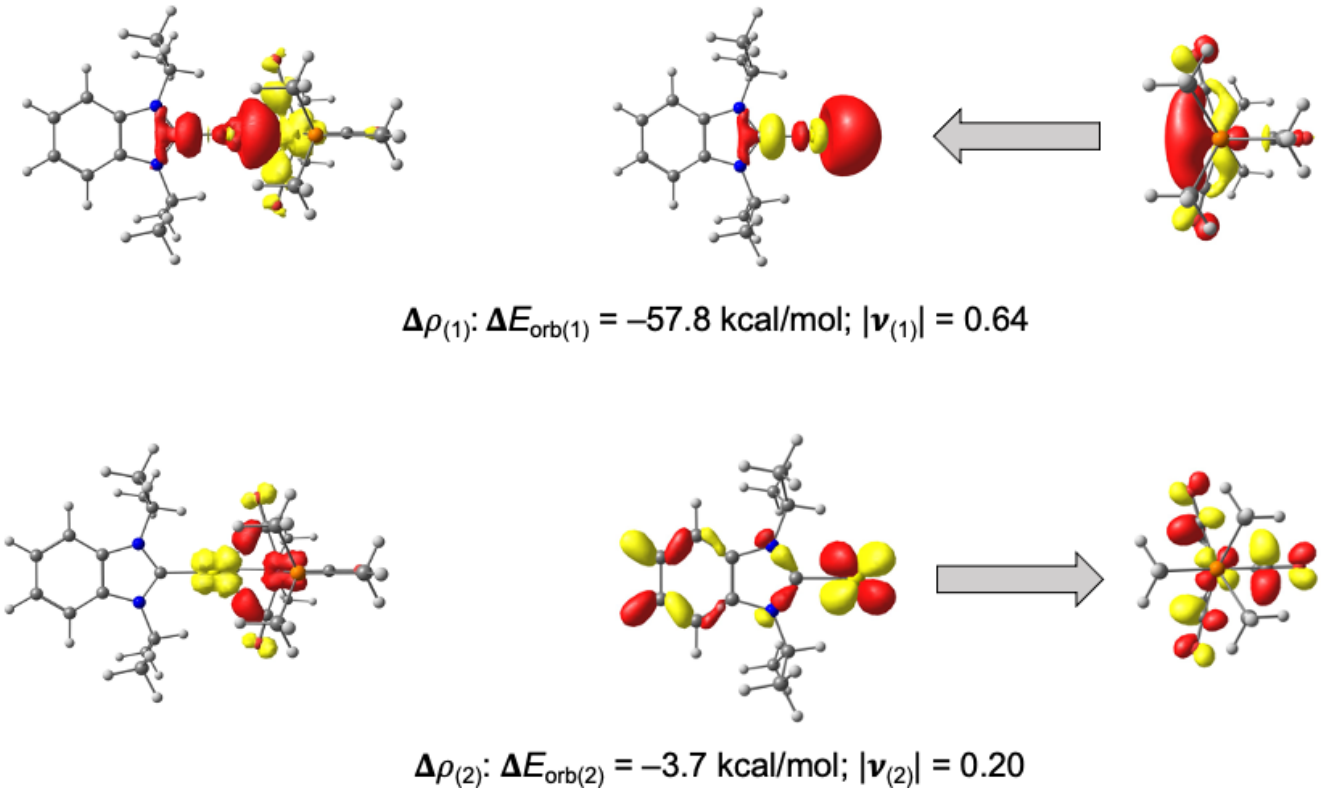

Figure S34. The shape of the deformation densities $\Delta_{(n)}$ (isosurface 0.003 a.u.) and corresponding canonical fragment orbitals (isosurface 0.05 a.u.) of $\{AuNHC\}^+$ and $Fe(CO)_3(PMe_3)_2$ in their singlet states at the B3LYP-D3(BJ)/def2-TZVPP level. The eigenvalues $|\nu_n|$ give the size of the charge migration in e. The direction of the charge flow of the deformation densities is yellow⟶red.

The lead term in the orbital interaction between the $[Au(NHC)]^+$ and $Fe(CO)_3(PMe_3)_2$ fragments is given by the $\Delta\rho_{(1)}$ interaction, which comprises $Fe(CO)_3(PMe_3)_2$ donation into the dominantly 6s/6p acceptor hybrid orbital of the Au^+ fragment. One smaller component $\Delta_{(2)}$ involving d backdonation from filled 5d AOs of Au^+ to vacant ligand molecular orbitals (MOs) is also shown.

Frontier Molecular Orbital Analysis

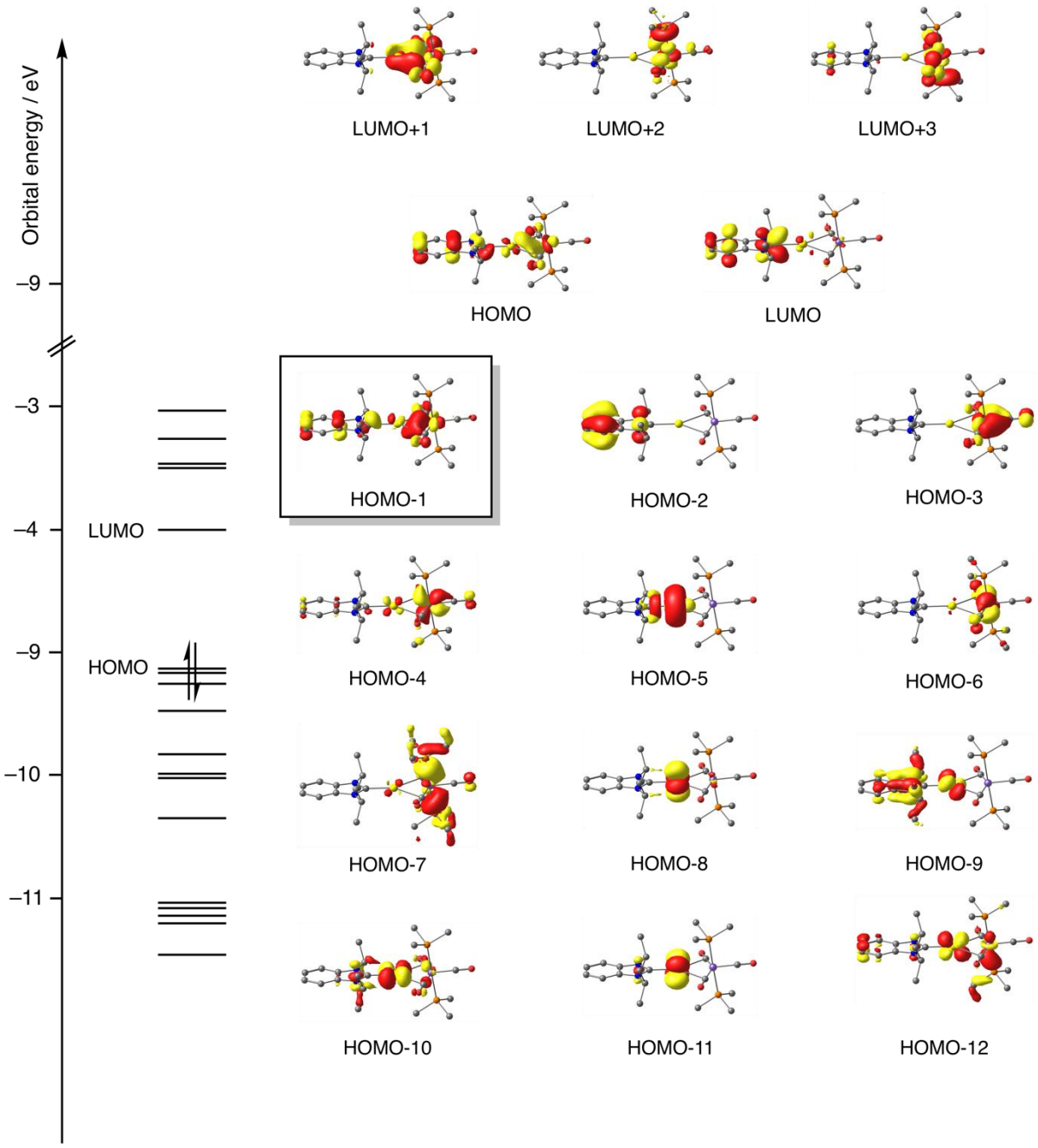

Figure S35. Molecular orbital diagram of the canonical Kohn-Sham frontier orbital region (isosurface 0.05 a.u.) at the B3LYP-D3(BJ)/def2-TZVPP level.

DLPNO-CCSDT(T) Local Energy Decomposition (LED) Analysis

The energy of a supermolecule **AB** relative to the total energies of the noninteracting fragments **A** and **B**, i.e. their binding energy, can be written as

$\Delta E = \Delta E_{\text{geo-prep}} + \Delta E_{\text{int}}$

where $\Delta E_{\text{geo-prep}}$ is the geometric preparation energy required to distort the fragment **A** and **B** from the relaxed structures as infinite separation to their geometry adapted in the supermolecule **AB**. The interaction energy ΔE_{int}, between fragments **A** and **B** frozen in the geometry they have in the adduct **AB** can be decomposed into a reference contribution and a correlation contribution such that

$\Delta E_{\text{int}} = \Delta E^{\text{ref}}_{\text{int}} + \Delta E^{\text{C}}_{\text{int}}$

By exploiting the localisation of the occupied orbitals withing the DLPNO framework, it is possible to discriminate between intra- and intermolecular contributions, hence allowing for further partitioning of the energy terms into several contributions

$\Delta E_{\text{int}} = \Delta E^{\text{ref}}_{\text{el-prep}} + E^{\text{ref}}_{\text{elstat}} + E^{\text{ref}}_{\text{exch}} + \Delta E^{\text{C-CCSD}}_{\text{non-dispersion}} + \Delta E^{\text{C-CCSD}}_{\text{dispersion}} + \Delta E^{\text{C-(T)}}_{\text{int}}$

Table S3. DLPNO-CCSD(T) binding energy of the dimer together with individual LED terms (kcal mol^{-1}).

	$[Au(NHC)]^+$	$Fe(CO)_3(PMe_3)_2$	total
ΔE			–66.7
Decomposition of ΔE			
$\Delta E_{\text{geo-prep}}$	+1.5	+7.5	+9.0
ΔE_{int}			–75.8
Decomposition of $\Delta E^{\text{ref}}_{\text{int}}$			
$\Delta E^{\text{ref}}_{\text{int}}$			–56.2
$\Delta E^{\text{ref}}_{\text{el-prep}}$	153.1	451.2	+604.3
$E^{\text{ref}}_{\text{elstat}}$			–547.5
$E^{\text{ref}}_{\text{exch}}$			–112.9
Decomposition of $\Delta E^{\text{C}}_{\text{int}}$			
$\Delta E^{\text{C}}_{\text{int}}$			–19.6
$\Delta E^{\text{C-CCSD}}_{\text{non-dispersion}}$			4.0
$\Delta E^{\text{C-CCSD}}_{\text{dispersion}}$			–24.2
$\Delta E^{\text{C-(T)}}_{\text{int}}$			0.6

The calculated dimerization energy (ΔE = –66.7 kcal mol^{-1}) is indicative of a strong interaction between the two fragments. The geometric preparation and perturbative triples do not make a significant contribution, whilst the largest contributions stem from the electronic preparation and electrostatic interactions in the

reference. The interfragment exchange energy (E^{ref}_{exch} = –112.9 kcal mol^{-1}) provides a substantial amount of the stabilisation component. London dispersion effects are also important ($\Delta E^{C\text{-}CCSD}_{dispersion}$,= –24.2 kcal mol^{-1}) in further stabilising the interaction between the fragment, amounting to nearly 33% of the total interaction energy.

References

[1] G. R. Fulmer, A. J. M. Miller, N. H. Sherden, H. E. Gottlieb, A. Nudelman, B. M. Stoltz, J. E. Bercaw, K. I. Goldberg, *Organometallics* **2010**, *29*, 2176.

[2] (a) T. Li, A. J. Lough, R. H. Morris, *Chem. Eur. J*. **2007**, *13*, 3796; (b) H. V. Huynh, Y. Han, J. H. H. Ho, G. K. Tan, *Organometallics* **2006**, *25*, 3267; (c) H. V. Huynh, Y. Han, R. Jothibasu, J. A. Yang, *Organometallics* **2009**, *28*, 5395; (d) L. Omann, M. Oestreich, *Organometallics* **2017**, *36*, 767; (e) R. Jothibasu, H. V. Huynh, L. L. Koh *J. Organomet. Chem.* **2008**, *693*, 374

[3] (a) A. D. Becke, *Phys. Rev. A* **1988**, *38*, 3098; (b) J. P. Perdew, *Phys. Rev. B* **1986**, *33*, 8822.

[4] (a) F. Weigend, R. Ahlrichs *Phys. Chem. Chem. Phys*., **2005**, *7*, 3297; (b) F. Weigend, M. Häser, H. Patzelt, R. Ahlrichs *Chem. Phys. Lett.* **1998**, *294*, 143.

[5] D. Andrae, U. Haussermann, M. Dolg, H. Stoll, H. Preuss *Theor. Chim. Acta*., **1990**, *77*, 123.

[6] K. Eichkorn, F. Weigend, O. Treutler, R. Ahlrichs *Theor. Chem. Acc*., **1997**, *97*, 119.

[7] S. Grimme, J. Antony, S. Ehrlich, H. Krieg, *J. Chem. Phys*., **2010**, *132*, 154104–1.

[8] Gaussian 16, Revision B.01, M. J. Frisch, G. W. Trucks, H. B. Schlegel, G. E. Scuseria, M. A. Robb, J. R. Cheeseman, G. Scalmani, V. Barone, G. A. Petersson, H. Nakatsuji, X. Li, M. Caricato, A. V. Marenich, J. Bloino, B. G. Janesko, R. Gomperts, B. Mennucci, H. P. Hratchian, J. V. Ortiz, A. F. Izmaylov, J. L. Sonnenberg, D. Williams-Young, F. Ding, F. Lipparini, F. Egidi, J. Goings, B. Peng, A. Petrone, T. Henderson, D. Ranasinghe, V. G. Zakrzewski, J. Gao, N. Rega, G. Zheng, W. Liang, M. Hada, M. Ehara, K. Toyota, R. Fukuda, J. Hasegawa, M. Ishida, T. Nakajima, Y. Honda, O. Kitao, H. Nakai, T. Vreven, K. Throssell, J. A. Montgomery, Jr., J. E. Peralta, F. Ogliaro, M. J. Bearpark, J. J. Heyd, E. N. Brothers, K. N. Kudin, V. N. Staroverov, T. A. Keith, R. Kobayashi, J. Normand, K. Raghavachari, A. P. Rendell, J. C. Burant, S. S. Iyengar, J. Tomasi, M. Cossi, J. M. Millam, M. Klene,

C. Adamo, R. Cammi, J. W. Ochterski, R. L. Martin, K. Morokuma, O. Farkas, J. B. Foresman, and D. J. Fox, Gaussian, Inc., Wallingford CT, 2016.

[9] F. Weinhold, C. Landis, Valency and Bonding, A Natural Bond Orbital Donor – Acceptor Perspective, Cambridge University Press, Cambridge, 2005.

[10] (a) NBO 6.0 (revision 18a), E. D Glendening, J. K. Badenhoop A. E. Reed, J. E. Carpenter, J. A. Bohmann, C. M. Morales, C. R. Landis, F. Weinhold (Theoretical Chemistry Institute, University of Wisconsin, Madison, WI, 2013), http://nbo6.chem.wsic.edu/ (b) E. D. Glendening, C. R. Landis, F. Weinhold *J. Comput. Chem*., **2013**, *34*, 1429.

[11] R. F. W. Bader, Atoms in Molecules: A Quantum Theory 1990, Clarendon Press, Oxford, 1990.

[12] AIMAll (Version 19.10.12), T. A. Keith, TK Gristmill Software, Overland Park KS, USA, 2019.

[13] P. Pollak, F. Weigend *J. Chem. Theory Comput*., **2017**, *13*, 3696.

[14] (a) W. B. Schneider, G. Bistoni, M. Sparta, M. Saitow. C. Riplinger, A. A. Auer, F. Neese *J. Chem. Theory Comput*., **2016**, *12*, 4778; (b) G. Bistoni *WIREs Comput. Mol. Sci*., **2020**, e1442.

[15] (a) M. P. Mitoraj, A. Michalak, T. Ziegler *J. Chem. Theory Comput*., **2009**, *5*, 962; (b) A. Altun, F. Neese, G. Bistoni *J. Chem. Theory Comput*., **2019**, *15*, 215.

[16] F. Neese *WIREs Comput. Mol. Sci*., **2022**, e1606.

[17] (a) A. D. Becke *J. Chem. Phys*., **1993**, *98*, 5648; (b) C. Lee, W. Yang, R. G. Parr *Phys. Rev. B*, **1988**, *37*, 785; (c) B. Miehlich, A. Savin, H. Stoll, H. Preuss, *Chem. Phys. Lett.* **1989**, *157*, 2006; (d) P. J. Stephens, F. J. Devlin, C. F. Chabalowski, M. J. Frisch *J. Phys. Chem*., **1994**, *98*, 11623.

[18] (a) F. Neese, F. Wennmohs, A. Hansen, U. Becker *Chem. Phys*., **2009**, *356*, 98; (b) B. Helmich-Paris, B. de Souza, F. Neese, R. Izsák *J. Chem. Phys*., **2021**, *155*, 104109.

[19] F. Weigend *Phys. Chem. Chem. Phys*., **2006**, *8*, 1057.

[20] (a) C. Riplinger, F. Neese *J. Chem. Phys*., **2013**, *138*, 034106; (b) C. Riplinger, B. Sandhoefer, A. Hansen, F. Neese *J. Chem. Phys*., **2013**, *139*, 134103; (c) C. Riplinger, P. Pinski, U. Becker, E. F. Valeev, F. Neese *J. Chem. Phys*., **2016**, 144, 024109.

[21] S. F. Boys *Rev. Mod. Phys*., **1960**, *32*, 296.